Chemical Geology 577 (2021) 120283

Contents lists available at ScienceDirect

Chemical Geology

journal homepage: www.elsevier.com/locate/chemgeo

Invited Research Article

Imprint of chemical weathering and hydrothermalism on the Ge/Si ratio and Si isotope composition of rivers in a volcanic tropical island, Basse-Terre, Guadeloupe (French West Indies)

François Gaspard [a], Sophie Opfergelt [a,*], Celine Dessert [b], Vincent Robert [b], Yolanda Ameijeiras-Mariño [a], Pierre Delmelle [a]

[a] Earth and Life Institute, Environnemental Sciences, Université catholique de Louvain, 1348 Louvain-la-Neuve, Belgium
[b] Université de Paris, Institut de Physique du Globe de Paris, CNRS, 75005 Paris, France

ARTICLE INFO

Editor: Dr. Don Porcelli

Keywords:
Chemical weathering
Si isotope
Ge/Si ratio
River geochemistry
Volcanic hydrothermal system
Guadeloupe

ABSTRACT

A significant portion of the disproportionally high chemical weathering flux in volcanic island arcs may originate from hydrothermal fluid-rock interaction, thereby compromising the accurate estimate of atmospheric CO_2 consumption rates. The objective of this study is to evaluate how the riverine Ge/Si ratio and Si isotopes, two well-established tracers of weathering, respond to hydrothermal inputs. The work took place in Basse-Terre, Guadeloupe, a tropical volcanic island with a dense river network, high chemical weathering fluxes and various hydrothermal surface manifestations. We characterized the Ge/Si ratio and $\delta^{30}Si$ of 15 thermal springs, nine non-impacted (NI) rivers and 13 hydrothermally-impacted (HI) rivers. The soil solution from a highly weathered soil profile (Ferralsol) and a clayey-rock corresponding to the material exposed in an extinct hydrothermal system were also measured. A new purification method was successfully developed in order to allow the reliable measurement of Si isotopes in SO_4^{2-}- and Cl^--rich thermal spring and HI river waters by mass spectrometry. Basse-Terre's thermal springs have variable Ge/Si ratios (0.05–21.03 $\mu mol.mol^{-1}$) and $\delta^{30}Si$ (0.71–1.50‰), but with no apparent relationship to the water compositional type. The Ge/Si ratio (0.15–2.57 $\mu mol.mol^{-1}$) and Si isotope composition (0.26–1.21‰) values of the NI rivers reveal differences in the watersheds' weathering degree. Dissolution of Ge- and ^{28}Si-rich secondary minerals explains the high Ge/Si and isotopically light composition of the northern NI rivers draining strongly weathered terranes. The Ge/Si ratio and $\delta^{30}Si$ values measured for the NI and HI rivers overlap, implying that they cannot be used to diagnose hydrothermal contributions to river basins unambiguously. However, when combined with the Cl^- and SO_4^{2-} concentrations, the analysis of Ge and Si in the HI rivers suggests that water seeping through an extinct hydrothermal system produces SO_4-rich drainages with distinctively lower Ge/Si ratios than those inferred for watersheds receiving thermal spring discharges associated with an active hydrothermal system. Overall, our results provide new constraints for applying and interpreting Ge/Si and Si isotope measurements to study weathering in volcanic environments.

1. Introduction

Continental silicate weathering rates are normally quantified by summing chemical weathering fluxes in rivers (e.g., Gaillardet et al., 1999). Knowledge of chemical weathering rates allows the estimate of atmospheric CO_2 consumption over different time periods (Berner et al., 1983; Raymo and Ruddiman, 1992; François and Walker, 1992). Recent studies highlight that weathering in volcanic island arcs with intermediate and felsic rock compositions is responsible for a disproportionately large contribution to global weathering budgets (e.g., Goldsmith et al., 2008, 2010; Jones et al., 2011; Schopka et al., 2011; Gaillardet et al., 2011; Blazina and Sharma, 2013). This is due in part to the high abundances of Ca and Mg silicates in arc terranes, the weathering of which results in high CO_2 consumption rates (e.g., Berner et al., 1983; François and Walker, 1992; Louvat and Allègre, 1997; Gaillardet et al., 1999; Dessert et al., 2003), but also to the mineralogy (olivine,

* Corresponding author.
E-mail address: sophie.opfergelt@uclouvain.be (S. Opfergelt).

https://doi.org/10.1016/j.chemgeo.2021.120283
Received 26 August 2020; Received in revised form 2 April 2021; Accepted 23 April 2021
Available online 27 April 2021

pyroxene, amphibole, glass) and texture (tephra) of volcanic arc-derived rocks which enhance dissolution reactions. Moreover, many of the active island arcs are located in the wet tropics where high runoff rates prevail (e.g., Vörösmarty et al., 2000; Gaillardet et al., 2011).

Chemical weathering rates are controlled by bedrock age, temperature, runoff, upflift/erosion rate and relief, among other variables (e.g., Lerman and Meybeck, 1988; White and Brantley, 1995; Gaillardet et al., 1999; Dixon et al., 2009). Volcanic island arcs usually display rock substrata that vary little in composition, but which can span a range of ages, depending on the eruptive history of the volcanic center(s). On Basse-Terre Island, Guadeloupe, previous studies (Gaillardet et al., 2011; Lloret et al., 2011; Dessert et al., 2015) demonstrated that highly weathered watersheds produce much lower weathering rates than rivers draining soils developed on younger bedrock. This reflects mainly the combined effect of bedrock ages and runoff.

Another feature of volcanic islands is that they often host various hydrothermal manifestations, including fumaroles, thermal springs and hot grounds, which are sustained by the cooling and degassing of a magma intrusion at depth. In these terranes, a significant portion of the chemical weathering fluxes is driven by hydrothermal fluid-rock interactions. For example, Rivé et al. (2013) concluded for the Lesser Antilles that up to 40% of the weathering flux is hydrothermal in origin. In the Philippines, Schopka et al. (2011) argued that on average approximately 10% of the dissolved cation load in rivers relates to hydrothermal activity. Other studies have demonstrated a substantial influence of hydrothermalism on weathering rates in La Réunion (Louvat and Allègre, 1997), Kamchatka, Russia (Dessert et al., 2009), Iceland (Louvat et al., 2008) and Yellowstone, USA (Hurwitz et al., 2010).

The acidity fueling hydrothermal fluid-rock interaction originates from the dissolution of magmatic volatiles, mainly CO_2, SO_2, H_2S and sometimes HCl, into the subsurface hydrothermal system (Henley and Ellis, 1983; Dessert et al., 2009; Hurwitz et al., 2010). However, sulfide minerals represent another potential source of acidity in hydrothermal systems, extinct or active. In particular, the oxidative dissolution of pyrite (FeS_2), a mineral commonly formed during hydrothermal alteration in sulfur-rich volcanic environments (Henley and Ellis, 1983), releases sulfuric acid during weathering. While potentially important, the contribution of this non-atmospheric source of acid to chemical weathering fluxes in volcanic terranes is largely unconstrained (Gaillardet et al., 2011; Rivé et al., 2013; Dessert et al., 2015). Clearly, a portion of the riverine solutes in active volcanic arc islands hosting active and extinct hydrothermal manifestations may originate from water-rock reactions driven by acids other than the carbonic acid derived from atmospheric CO_2. Thus, besides recognizing that bedrock age exerts a strong control on weathering in volcanic island arcs, the hydrothermal influence on chemical weathering fluxes should be constrained in order to assess accurately the contribution of these tectonic settings to global atmospheric CO_2 consumption.

The concentrations and isotope compositions of mobile elements, including C, Sr, U—Th and B have been used to decipher a hydrothermal contribution to rivers in volcanic terranes (Louvat and Allègre, 1997; Gaillardet et al., 2011; Rad et al., 2011; Louvat et al., 2011; Rivé et al., 2013). However, these tracers fail to distinguish chemistry fluxes originating from catchments with contrasted weathering degrees. In contrast, when applied in combination, Si isotopes and Ge/Si ratio measurements can track the weathering processes that underpin dissolved chemical fluxes (e.g., Derry et al., 2005; Ziegler et al., 2005; Opfergelt et al., 2010, 2013; Kurtz et al., 2011; Aguirre et al., 2017; Ameijeiras-Mariño et al., 2018; Baronas et al., 2018; Baronas et al., 2020). However, the few Si isotope (Douthitt, 1982; Opfergelt et al., 2011; Geilert et al., 2015; Ding et al., 2017; Chen et al., 2020) and Ge/Si ratio (Arnòrsson, 1987; Siebert et al., 2006; Escoube et al., 2015) data available for volcanic thermal springs suggest that the addition of hydrothermal fluids to rivers can blur the isotopic and chemical signatures inherited from low-temperature weathering reactions.

Basse-Terre Island, Guadeloupe, French West Indies, is a prime location to study weathering and hydrothermal contribution to rivers because (i) the lithology is largely invariant across the island (Westercamp, 1988; Boudon et al., 2008; Samper et al., 2007, 2009), (ii) there is a clear south to north weathering gradient (Colmet-Daage and Lagache, 1965; Colmet-Daage, 1969; Cabidoche et al., 2009; Gaillardet et al., 2011; Lloret et al., 2011; Dessert et al., 2015), (iii) the island hosts both active and extinct hydrothermal systems (Verati et al., 2014, 2018; Favier et al., 2019; Salaün et al., 2011), and (iv) the geochemistry of the thermal springs and rivers are well-described (e.g., Brombach et al., 2000; Villemant et al., 2005; Gaillardet et al., 2011; Lloret et al., 2011; Villemant et al., 2014; Dessert et al., 2015). Here, we report the Si isotope composition and Ge/Si ratio of thermal springs and rivers in Basse-Terre, Guadeloupe. Our objectives are (i) to develop and apply a protocol to measure Si isotopes in anion- and cation-rich thermal springs and river waters affected by hydrothermal discharges, (ii) to document the $\delta^{30}Si$ and Ge/Si ratio variability in thermal springs that vary in composition, (iii) to assess the capability of $\delta^{30}Si$ and Ge/Si ratios to record hydrothermal inputs to rivers, and (iv) to confirm the suitability of $\delta^{30}Si$ and Ge/Si ratio determinations for tracing low-temperature weathering processes in volcanic terranes with hydrothermal surface manifestations.

2. Geological, pedological and climatic setting

Basse-Terre Island (950 km^2; 16°N, 61°W) is located in the Guadeloupe archipelago, Lesser Antilles, Caribbean Sea (Fig. 1). Basse-Terre consists of four main volcanic massifs varying in composition from basaltic-andesite to andesite (e.g., Samper et al., 2007, 2009; Boudon et al., 2008; Ricci et al., 2017; Favier et al., 2019). The oldest massifs are found in north Basse-Terre and include the Basal Complex (4.30–2.68 Ma) and the Septentrional Chain (1.81–1.15 Ma). Younger volcanism in the southern part of the island formed the Axial Chain (1.02–0.44 Ma) and the La Grande Découverte-La Soufrière composite volcano (445–205 ka to present). The Amic crater, which lies within the La Grande Découverte Caldeira, hosts the andesitic dome of La Soufrière (1464 m above sea level; Fig. 1). The lava dome was emplaced at the end of the last magmatic eruptive activity in 1530 CE (Boudon et al., 2008). Extinct hydrothermal systems, such as those found at Deshaies Dome, Les Mamelles Complex, Bouillante, and Carmichaël, are associated to old volcanic centers occurring in the main volcanic massifs (Basal Complex, Septentrional Chain, Axial Chain, La Grande Découverte complex, respectively; Verati et al., 2014, 2018; Favier et al., 2019; Salaün et al., 2011; Fig. 1).

Numerous fumaroles, thermal springs and temperature anomalies at the summit and periphery of the lava dome reveal the presence of an active hydrothermal system centered on La Soufrière (Brombach et al., 2000). This shallow aquifer (~500 m below the surface), delimited by the Amic caldera border, has an estimated temperature of 190–260 °C. It is fed by meteoric water percolating through pyroclastic deposits and by hot magmatic fluids (Brombach et al., 2000). The distribution of thermal springs on La Soufrière is controlled by several fracture systems, where intense hydrothermal alteration of the andesitic rocks takes place (Nicollin et al., 2006; Zlotnicki et al., 2006; Rosas-Carbajal et al., 2016). Thermal springs are also found around extinct hydrothermal systems, for example in the Bouillante geothermal area. Several studies have described the geochemistry of Basse-Terre's thermal springs (e.g., Bigot and Hammouya, 1982; Brombach et al., 2000; Louvat et al., 2011; Ruzié et al., 2013; Villemant et al., 2014; Dessert et al., 2015).

Basse-Terre Island has a dry-winter tropical climate, with annual temperature and relative humidity averaging to ~23 °C and 75%, respectively (MétéoFrance, 2019). The dry and rainy seasons run from January to April and from June to November, respectively. The average annual precipitation (between 1981 and 2010; MétéoFrance, 2019) fluctuates between 1050 and 8500 mm yr^{-1}, depending on relief. This large variation reflects an orographic effect; the east coast receives high rainfall due to the strong influence of the Easterly and conversely, the

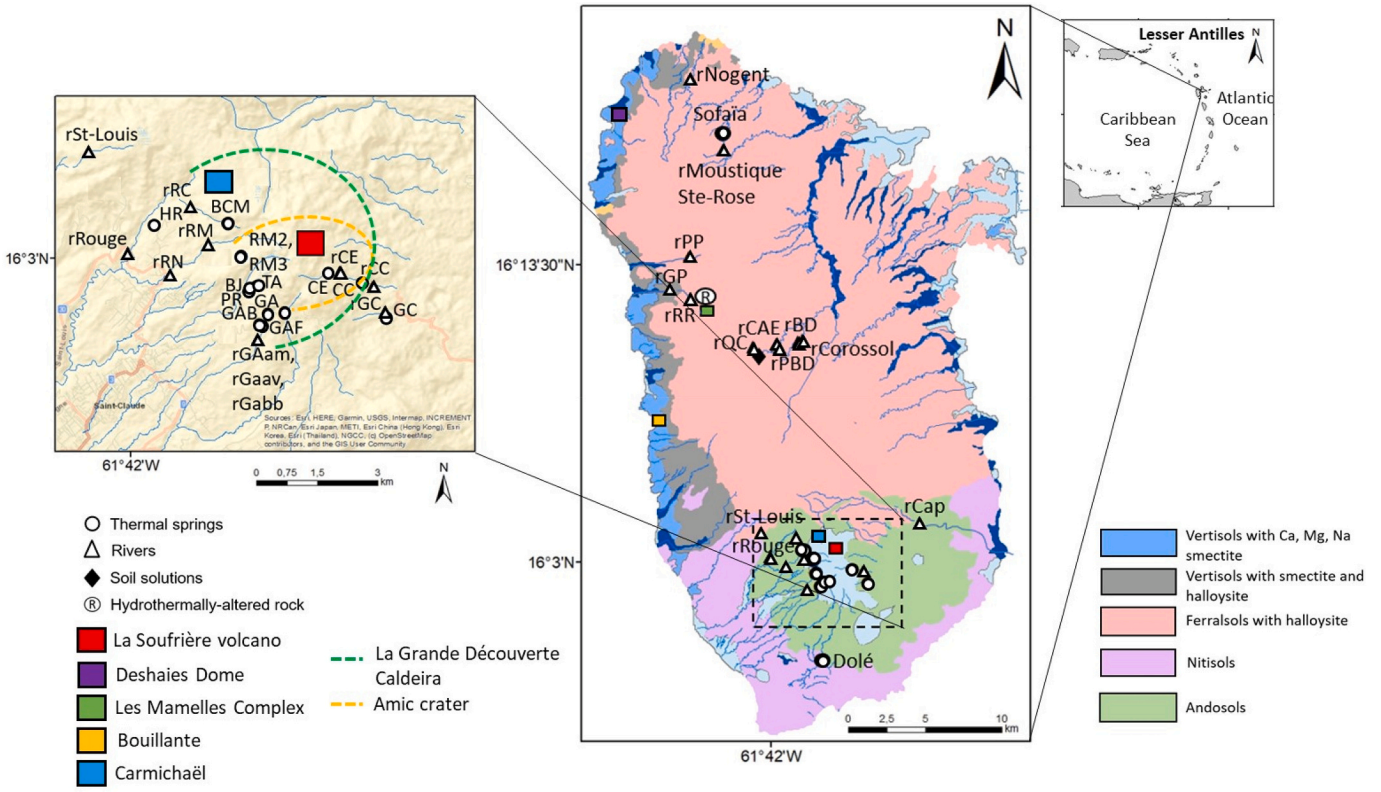

Fig. 1. Sampling locations on Basse-Terre Island, Guadeloupe, Lesser-Antilles. The thermal springs (open circle), rivers (open triangle), soil solutions (black diamond) and hydrothermally-altered rock (®) are depicted on a simplified soil map (modified from Cabidoche, 2011). Also shown are La Soufrière volcano, Deshaies Dome, Les Mamelles Complex, Bouillante geothermal area and Carmichaël. The approximate boundaries of the La Grande Découverte caldeira and Amic crater are represented by dotted lines (Komorowski et al., 2005; Barat, 1986). All the sample codes are described in Table 1. (2 column fitting image).

west coast, protected by the orographic barrier, receives less rainfall (Chaperon et al., 1985). Combined with the rugged and steep relief of Basse-Terre, the abundant rainfall feeds a dense river network. There are 30 and 25 independent river systems on the west and east coasts of Basse-Terre, respectively, all with a watershed area greater than 1 km^2 (DIREN; French Water Survey agency). Gaillardet et al. (2011), Lloret et al. (2011) and Dessert et al. (2015) provide a detailed description of the river geochemistry. They emphasize that the chemical composition of river waters is strongly influenced by the amount of rainfall, hydrothermal alteration (extinct and active systems) and water-mineral interactions during chemical weathering processes. Depending on location, the river systems drain terrains with contrasted soil properties. Highly-weathered soils, which include clay mineral-rich Ferralsols and Vertisols are found in the northern and central parts of Basse-Terre (Fig. 1), where Pliocene volcanic deposits dominate the landscape (Colmet-Daage, 1969). In contrast, young and less weathered Andosols derived from Quaternary volcanic deposits occur in the south of the island.

3. Material and methods

3.1. Sampling

Fifteen thermal springs were sampled on Basse-Terre Island between 2015 and 2018 (Fig. 1; Table 1). Most of these springs have been monitored routinely by the Observatoire Volcanologique et Sismologique de la Guadeloupe-Institut de Physique du Globe de Paris (OVSG-IPGP) since 1978. The springs Ravine Marchand (RM2 and RM3), Galion (GA), Galion Blanc (GAB), Galion Froid (GAF), Carbet-Echelle (CE), Bains Jaunes (BJ), Pas du Roy (PR) and Tarade (TA) sit inside the Amic Crater at elevations ranging from ~980 to 1150 m. Grosse Corde (GC) and Chute du Carbet (CC) lie farther away from the lava dome on the eastern side of the volcano, whereas Bains Chauds du Matouba (BCM) and Habitation Revel (HR) are located on its western flank. Dolé is a thermal spring located ~5.8 km to the south of La Soufrière. We also sampled a thermal spring (Sofaïa) in the northern part of the island. We did not include thermal springs from the Bouillante geothermal area in our study as these are contaminated by seawater (Brombach et al., 2000).

Water samples from 22 rivers were obtained in January–February 2015, October–November 2017 and April 2018 (Table 1). The river samples were collected as much as possible from areas with minimum anthropogenic disturbances. The rivers drain watersheds in the north (n = 5; rivière Nogent (rNogent), Moustique Ste-Rose (rMoustique Ste-Rose), Petite Plaine (rPP), Grande Plaine (rGP) and Ravine Rouge (rRR)), the center (n = 5; Corossol (rCorossol), Bras David (rBD), Quiock Creek (rQC), Cascade aux écrevisses (rCAE), Petit Bras David (rPBD)), and the south of Basse-Terre (n = 3; Ravine Marchand (rRM), Ravine Chaude (rRC) and Galion (rGA). Water samples from rGA were obtained from three locations: "amont" (rGAam), "aval" (rGAav) and "bassin bleu" (rGAbb). Three rivers were sampled on the west coast (Noire (rRN), St-Louis (rSt-Louis) and Rouge (rRouge)) and fours rivers on the east coast (n = 4; Capesterre (rCap), Chute du Carbet (rCC), Carbet (rCE), Grosse Corde (rGC)) of South Basse-Terre (Fig. 1). The rPP, rGP, and rRR rivers drain the extinct hydrothermal system associated with Les Mamelles, and the rRouge river drains the extinct hydrothermal system of Carmichaël. The thermal spring BCM is in the watershed of rRC river, the springs RM2 and RM3 are in the watershed of rRN river, the Galion springs (GA, GAB, GAF) are in the watershed of rGA river, the springs CE and CC are in the watershed of Carbet river (rCE and rCC) and the spring GC is in the watershed of rGC river. Several of these rivers (rBD, rQC, rPBD, rSt-Louis, rRouge and rCap) have been monitored

Table 1
Description and compositions of the thermal springs, river waters and soil solutions as sampled in 2015, 2017 and 2018. Eleven springs and seven rivers were collected several times on different dates. The thermal springs are sorted by type, following Brombach et al. (2000)'s classification (see text). The river water samples are sorted by their positioning on Basse-Terre from North to South. Rivers affected by hydrothermal inputs are denoted by "HI".

Sample	Code	Sampling date	Type	Temperature	pH	Conductivity	Alkalinity	Ca	Na	Mg	K	Al	Fe	Si	SO_4	Cl
		dd.mm.yy		°C		µs.cm^{-1}	µmol.l^{-1}									
Thermal springs																
Ravine Marchand 2	RM2(1)	27.01.15	$Ca\text{-}SO_4$ water	21.5	3.3	549	0	1268	589	442	68	226	54	1375	2291	813
Ravine Marchand 2	RM2(2)	12.10.17	$Ca\text{-}SO_4$ water	21.6	3.6	711	0	1863	696	602	75	167	54	1449	2697	1336
Ravine Marchand 3	RM3(1)	27.01.15	$Ca\text{-}SO_4$ water	41.1	5.5	1360	1900	4029	1948	1605	384	n.d	208	2585	4281	3960
Ravine Marchand 3	RM3(2)	12.10.17	$Ca\text{-}SO_4$ water	43.3	5.3	1581	2043	4416	2221	1765	431	n.d	253	2882	4788	5141
Carbet-Echelle	CE(1)	17.11.17	$Ca\text{-}SO_4$ water	21.0	5.3	1442	883	5115	1170	1646	148	16	1200	1735	8136	301
Carbet-Echelle	CE(2)	15.03.18	$Ca\text{-}SO_4$ water	20.9	5.3	1469	1001	5217	1196	1655	148	17	1170	1744	8752	315
Galion	GA(1)	29.01.15	$Ca\text{-}SO_4$ water	48.0	4.6	2040	603	6635	2545	2623	492	1	287	2882	6638	7930
Galion	GA(2)	14.11.17	$Ca\text{-}SO_4$ water	48.6	4.8	1909	599	5649	2184	2136	454	3	275	2669	6281	7194
Galion Blanc	GAB(1)	29.01.15	$Ca\text{-}SO_4$ water	42.8	4.6	1844	499	5692	2455	2546	444	7	111	2607	5842	7295
Galion Blanc	GAB(2)	14.11.17	$Ca\text{-}SO_4$ water	44.1	4.8	1795	502	5414	2364	2369	416	5	159	2721	5568	7793
Galion Froid	GAF	29.01.15	$Ca\text{-}SO_4$ water	21.7	4.5	304	194	905	485	281	55	26	4	1491	1211	517
Bains Jaunes	BJ(1)	29.01.15	$Ca\text{-}SO_4$ water	29.2	4.9	706	181	1935	1334	786	133	3	n.d	1853	2734	1132
Bains Jaunes	BJ(2)	14.11.17	$Ca\text{-}SO_4$ water	29.6	5.2	673	194	1819	1290	710	128	4	n.d	1825	2497	958
Pas du Roy	PR(1)	29.01.15	$Ca\text{-}SO_4$ water	34.1	5.4	994	677	2706	2008	1306	267	n.d	42	2095	3898	1641
Pas du Roy	PR(2)	14.11.17	$Ca\text{-}SO_4$ water	33.9	5.7	980	661	2622	1997	1272	230	n.d	42	2080	3559	1537
Tarade	TA(1)	29.01.15	$Ca\text{-}SO_4$ water	42.0	5.5	1574	1292	4276	3796	2210	485	n.d	n.d	2384	6076	3393
Tarade	TA(2)	14.11.17	$Ca\text{-}SO_4$ water	43.5	5.8	1693	1405	4693	3941	2294	515	n.d	n.d	2533	6155	3841
Sofaïa	Sofaïa	02.02.15	$Ca\text{-}SO_4$ water	29.3	3.8	165	0	97	435	69	25	34	5	565	358	422
Bain Chaud du Matouba	BCM(1)	30.01.15	$Ca\text{-}SO_4$ water	58.5	5.9	1183	348	6629	1551	521	208	n.d	n.d	557	7491	573
Bain Chaud du Matouba	BCM(2)	20.10.17	$Ca\text{-}SO_4$ water	58.3	5.6	1362	391	6595	1610	537	208	1	n.d	566	7759	577
Chute du Carbet	CC(1)	28.01.15	Ca-Na-Cl water	43.0	6.7	935	2395	1698	2949	1218	438	n.d	n.d	1678	847	278
Chute du Carbet	CC(2)	07.11.17	Ca-Na-Cl water	42.0	6.7	852	2577	1608	2636	1117	393	n.d	n.d	1651	847	214
Grosse corde	GC(1)	28.01.15	Ca-Na-Cl water	38.3	6.3	1383	2399	2801	4047	1790	522	n.d	n.d	1576	2272	4749
Grosse corde	GC(2)	07.11.17	Ca-Na-Cl water	37.5	6.5	1640	2522	2590	3727	1651	495	n.d	n.d	1477	2489	4468
Habitation Revel	HR	20.10.17	Ca-Na-HCO_3 water	32.6	6.5	254	2098	484	1020	209	91	n.d	n.d	1284	175	241
Dolé	Dolé	04.02.15	Ca-Na-HCO_3 water	30.8	8.3	555	3248	1293	1690	903	174	n.d	n.d	1415	843	870

Sample	Code	Sampling date	Type	Temperature	pH	Conductivity	Alkalinity	Ca	Na	Mg	K	Al	Fe	Si	SO_4	Cl
		dd.mm.yy		°C		µs.cm^{-1}	µmol.l^{-1}									
River waters																
North Basse-Terre																
Nogent	rNogent	02.02.15		23.8	7.6	144	540	162	668	127	47	5	1	538	64	561
Moustique Sainte-Rose	rMoustique Ste-Rose	02.02.15		23.3	6.5	85	233	100	387	78	20	4	2	287	39	414
Petite Plaine	rPP	03.02.15	HI	23.4	7.5	169	893	302	541	182	31	2	0	546	95	410
Grande Plaine	rGP	27.04.18	HI	23.3	6.1	–	–	761	1044	546	50	4	2	560	741	401
Ravine Rouge	rRR	27.04.18	HI	23.4	4.2	–	0	435	482	237	29	3	4	560	1441	346
Central Basse-Terre																
Corossol	rCorossol	05.02.15		22.9	7.7	69	416	125	322	64	16	1	n.d	408	12	221
Bras David	rBD1	05.02.15		22.7	7.2	83	443	132	362	82	20	1	n.d	429	42	308
Bras David	rBD2	03.10.17		25.7	7.6	77	410	107	311	73	24	1	0	391	17	278
Bras David	rBD3	19.10.17		23.7	7.5	83	412	102	299	69	25	1	0	370	15	263
Bras David	rBD4	10.11.17		23.5	7.5	71	381	106	295	69	22	1	1	360	20	260
Quiock Creek	rQC1	05.02.15		23.1	4.8	46	–	11	274	31	4	2	n.d	89	13	318
Quiock Creek	rQC2	03.10.17		25.1	5.7	46	56	11	246	31	12	2	1	71	9	330
Quiock Creek	rQC3	19.10.17		24.6	5.5	48	43	12	241	29	15	2	1	69	21	323
Quiock Creek	rQC4	10.11.17		23.9	5.4	42	68	13	242	30	13	5	2	76	11	290
Cascade aux Ecrevisses	rCAE	04.02.15		24.9	8.2	137	433	122	450	75	20	1	n.d	373	23	409

(*continued on next page*)

Table 1 (*continued*)

Sample	Code	Sampling date	Type	Temperature	pH	Conductivity	Alkalinity	Ca	Na	Mg	K	Al	Fe	Si	SO_4	Cl
		dd.mm.yy		°C		µs.cm^{-1}	µmol.l^{-1}									
Petit Bras David	rPBD1	05.02.15		22.8	7.2	80	291	106	362	74	21	1	n.d	388	21	278
Petit Bras David	rPBD2	03.10.17		24.5	7.2	75	276	86	318	68	29	1	1	360	35	317
Petit Bras David	rPBD3	10.11.17		23.2	7.1	70	297	89	305	66	25	2	1	331	35	295
South Basse-Terre																
Ravine Marchand	rRM	27.01.15	HI	22.8	4.0	585	1370	1813	780	607	107	139	45	1451	2452	1347
Capesterre	rCap1	29.01.15		21.7	7.8	62	408	134	247	56	15	n.d	n.d	428	23	150
Capesterre	rCap2	27.10.17		22.5	7.3	41	489	68	157	33	20	1	0	211	17	139
Ravine Chaude	rRC1	30.01.15	HI	18.8	6.9	197	267	570	361	117	38	n.d	n.d	491	645	178
Ravine Chaude	rRC2	20.10.17	HI	20.5	7.2	128	295	327	265	84	29	1	n.d	445	373	168
Ravine Chaude	rRC3	24.01.18	HI	18.9	7.0	126	285	277	252	72	21	0	0	444	307	157
Chute du Carbet	rCC	28.01.15	HI	22.1	7.6	221	358	620	488	275	61	1	1	657	2018	2434
Rivière Carbet	rCE	17.11.17	HI	20.9	5.5	750	–	2620	674	735	86	1	808	1442	4573	211
Rivière Noire	rRN	27.01.15	HI	21.2	7.5	429	352	1290	944	556	138	1	n.d	1239	1649	1055
Saint-Louis	rSt-Louis1	30.01.15		22.9	7.1	106	690	222	340	113	27	n.d	n.d	543	51	193
Saint-Louis	rSt-Louis2	20.10.17		22.6	7.4	82	639	164	272	89	29	0	n.d	474	35	189
Rivière Rouge	rRouge1	30.01.15	HI	19.1	4.0	176	67	347	278	95	22	70	1	608	643	132
Rivière Rouge	rRouge2	20.10.17	HI	20.8	4.7	133	43	267	243	83	27	37	1	538	495	145
Rivière Rouge	rRouge3	26.01.18	HI	19.2	4.6	133	27	269	247	81	19	47	1	556	519	141
Grosse Corde	rGC	28.01.15	HI	31.5	7.3	983	1937	2305	3417	1494	443	1	n.d	1245	2720	5643
Rivière Galion amont	rGAam	29.01.15	HI	26.6	4.8	645	–	2218	1054	854	156	78	30	1755	2598	2365
Rivière Galion aval	rGAav	29.01.15	HI	28.2	5.1	848	110	3084	1370	1180	223	42	72	1947	3403	3483
Rivière Galion Bassin Bleu	rGAbb	30.01.15	HI	20.9	6.5	478	173	1576	883	623	94	2	n.d	1124	1551	2051
Soil solutions	Soil depth	Sampling date		Temperature	pH	Conductivity	Alkalinity	Ca	Na	Mg	K	Al	Fe	Si	SO_4	Cl
	cm	dd.mm.yy		°C		µs.cm^{-1}	µmol.l^{-1}									
GBD2–61	61	10.11.17		–	5.0	–	–	8	170	30	4	10	n.d	83	19	230
GBD2–91	91	10.11.17		–	5.6	–	–	6	241	31	4	4	n.d	96	14	278
GBD2–152	152	10.11.17		–	5.1	–	–	2	199	30	2	7	n.d	63	13	239
GBD2–274	274	10.11.17		–	4.8	–	–	1	208	29	3	10	n.d	70	14	289
GBD2–344	344	10.11.17		–	4.2	–	–	2	195	26	9	8	n.d	62	20	254
GBD2–457	457	10.11.17		–	5.0	–	–	10	198	19	6	6	n.d	116	14	217
GBD2–823	823	10.11.17		–	4.8	–	–	1	232	15	12	1	n.d	106	18	268

-: not measured; n.d: not detected.

routinely by the Observatoire de l'Eau et de l'Erosion-Institut de Physique du Globe de Paris (OBSERA-IPGP) since 2006.

The temperature, pH and conductivity (µS.cm^{-1}, referenced to 25 °C) of the thermal springs and rivers were measured in situ with a Hanna HI 991300 electrode. The water samples were filtered within 24 h after collection using 0.45 µm polycarbonate membranes, and then stored at 4 °C in the dark in pre-washed polypropylene bottles. An aliquot filtered and acidified to 0.5% *v*/v with suprapure HNO_3 was used for major, trace element and Si isotope analysis. The anions were measured on a separate unacidified sample aliquot.

Soil solutions were collected from a soil profile (GBD2 in Table 1) from the Quiock Creek catchment, which is monitored regularly by OBSERA. The soil is a Ferralsol, a soil group commonly encountered in the north and center of Basse-Terre and which is characterized by an advanced stage of weathering (Fig. 1). The soil solutions were retrieved at depths of 61, 91, 152, 274, 344, 457 and 823 cm using no-suction 5-cm diameter nested lysimeters equipped with porous ceramic cups (Buss et al., 2010; Clergue et al., 2015). The solutions were filtered with 0.45 µm polycarbonate filters prior to storage at 4 °C.

Finally, a sample of clayey, hydrothermally-altered rock collected from the Grande Plaine watershed which drains the extinct hydrothermal system of Les Mamelles (Fig. 1) was determined by X-ray powder diffraction (XRD, Bruker D8 Advance, Cu Kα, $I = 0.15418$ nm, 40 kV, 30 mA, $2\theta = 1°$/min). The analysis revealed the presence of pyrite, pyrophyllite and dickite, with minor smectite and residual feldspar in this sample (Appendix A).

3.2. Water composition analysis

The concentrations of Ca, Na, Mg, K, Al, Fe and Si in the water samples were determined by inductively-coupled plasma-optical emission spectrometry (ICP-OES; iCAP 6500 Thermo Fisher Scientific). The accuracy (< 0.5%) on the element concentration measurements was assessed by using the water reference material SLRS-5 (Yeghicheyan et al., 2013). The detection limits are 0.05, 0.43, 0.21, 0.26, 0.37, 0.18, 0.36 µmol.l^{-1} for Ca, Na, Mg, K, Al, Fe and Si respectively. The anions (SO_4^{2-}, Cl^-) were measured by ion chromatography (Dionex ICS2000, column: AG15/AS15). The accuracy for SO_4^{2-} and Cl^- is <2% and the detection limits are 1.5 and 3.1 µmol.l^{-1} for SO_4^{2-} and Cl^-, respectively. Alkalinity (µmol.l^{-1}) was determined on the same day as sampling using an automatic titrator (Metrohm 916 Ti-Touch titrator). In all cases, the charge balance of the water analyses never exceeds 10%.

3.3. Measurement of dissolved Ge concentration

The Ge concentration in all thermal springs, river waters, soil solutions and hydrothermally-altered rock was determined by ICP-mass spectrometry (ICP-MS, ICAPQ Thermo Fisher Scientific) with a PFA nebulizer of 400 µl.min^{-1} uptake rate, a quartz cyclonic spray chamber, and in 2% HNO_3. The three isotopes ^{72}Ge, ^{73}Ge and ^{74}Ge were monitored during Ge concentration analyses, and the most abundant isotope ^{74}Ge, was used for the measurement given the higher sensitivity and the lower detection limit compared to other isotopes (Delvigne et al., 2018). Rhodium was used as an internal standard to correct for instrumental drift. The typical ^{74}Ge sensitivity was 22,000 cps per µg.l^{-1} and ^{103}Rh sensitivity was 100,000 cps per µg.l^{-1}. Prior to analysis, the hydrothermal-altered rock was dissolved by alkaline fusion with 99.99% pure NaOH at 720 °C in a silver crucible (Georg et al., 2006). Thermal waters were diluted with MilliQ water to reach total dissolved solids <0.2% and ensuring Ge concentrations above detection limit. Accuracy and long-term repeatability of the analysis were assessed by measuring two international riverine standards, namely SLRS-5 ([Ge] = 0.083 ± 0.014 nmol.l^{-1}, SD; $n = 3$) and SLRS-6 ([Ge] = 0.097 ± 0.007 nmol.l^{-1}, SD; n = 3) in line with the published values (SLRS-5: 0.151 ± 0.151 nmol.l^{-1}, $n = 34$; SLRS-6: 0.138 ± 0.096 nmol.l^{-1}, $n = 45$; Yeghicheyan et al., 2013; Yeghicheyan et al., 2019), and the USGS rock standard BHVO-2 ([Ge] = 22.30 ± 0.89 nmol.l^{-1}, SD; n = 3) in agreement with the reported value (22.30 ± 0.55 nmol.l^{-1}, $n = 10$; Jochum et al., 2016). The GAB thermal spring ([Ge] = 23.95 ± 0.096 nmol.l^{-1}, SD; $n = 14$) was used as an in-house standard. The reference materials and the in-house standard were measured in each of the analytical sessions that took place between July 2017 and June 2018. The detection limit for Ge is 0.04 nmol.l^{-1} and the analytical precision of the measurement is ±8% for Ge concentrations <0.013 nmol.l^{-1} and ± 4% for Ge concentrations >0.013 nmol.l^{-1}. The standard deviation of our Ge/Si ratio determinations is 10%.

The measurement of dissolved Ge is usually performed by High Resolution ICP-MS (HR-ICP-MS) (Mortlock and Froelich, 1996; Hamade et al., 2003; McMahon et al., 2006; Frei and Polat, 2007; Delvigne et al., 2009; Cornelis et al., 2010; Tribovillard et al., 2011). Therefore, we compared the Ge concentrations in 12 thermal spring and 17 river water samples from Basse-Terre as measured by both HR-ICP-MS and ICP-MS (Appendix B). The HR-ICP-MS analyses of Ge (noted Ge*) were performed at the Department of Earth and Atmospheric Sciences, Cornell University, USA, using a Thermo Fisher Scientific-Element2™ Series instrument equipped with a hydride generation system, and applying the isotope dilution technique (Mortlock and Froelich, 1996). The Si concentrations used for calculating the Ge*/Si (HR-ICP-MS) and Ge/Si (ICP-MS) ratios (µmol.mol^{-1}) were determined by ICP-OES. Fig. 2 shows a strong correlation ($R^2 = 0.99$) between the Ge/Si ratio and Ge*/Si ratio measurements, indicating the validity of our ICP-MS analysis for determining the concentration of Ge in solution.

3.4. Silicon isotope measurements

3.4.1. Purification of anion-rich samples

The method commonly applied to purify solutions prior to the determination of the isotope composition of dissolved Si involves the removal of cations from the matrix using a single step cation-exchange resin (Georg et al., 2006). However, this method does not remove anions from the aqueous solution, potentially leading to matrix effects and analytical mass bias during measurements by Multi-Collector Inductively Coupled Plasma Mass Spectrometry (MC-ICP-MS) and using the sample-standard bracketing technique (van den Boorn et al., 2009; Hughes et al., 2011). Anions in solution can be partly removed by co-precipitating Si with molybdate using the triethylamine (TEA) molybdate method, followed by dissolution of the silica precipitate in HF (De La Rocha et al., 1996). A pre-concentration step, the magnesium-induced coprecipitation (MAGIC) method, is usually applied prior to the analysis of low-Si solution (Si (< 10 µmol l^{-1}) (Brzezinski et al., 2003). The MAGIC method also removes some of the dissolved anions. When the anion-to-Si ratio of the sample to be analyzed is low (SO_4^{2-}/Si

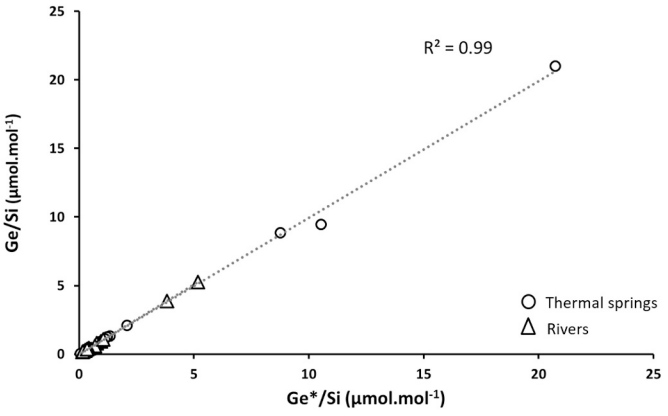

Fig. 2. Plot comparing the Ge/Si ratio (µmol.l^{-1}) of 12 thermal springs ($n = 12$) and 17 river waters from Basse-Terre as measured by ICP-MS and HR-ICP-MS (Ge*/Si). See text for explanation. (Single column fitting image).

mass ratio < 0.7; Cl^-/Si mass ratio < 1.1), doping both the sample and the standard with anions is sufficient to correct for the mass bias during the isotopic analysis carried out via the sample-standard bracketing technique (Hughes et al., 2011). However, this condition is not fulfilled in thermal waters as these often contain high concentrations of dissolved SO_4^{2-}, and sometimes Cl^-. In this case, a purification step is necessary prior to the measurement (van den Boorn et al., 2009). The TEA and MAGIC methods are relatively labor-intensive and have drawbacks. The use of HF in the former may lead to the loss of volatile SiF_4(g) during sample introduction, and thereby to unwanted Si isotope fractionation (Georg et al., 2006). Isotope fractionation may also be problematic when the recovery of Si at the end of the MAGIC pre-concentration step is incomplete. Moreover, MAGIC is performed at pH > 10 and bringing acidic thermal waters to such basic pH values is often accompanied by the formation of various Fe- and Al-(oxy)hydroxide precipitates.

Here we describe a new purification method, comprised of two steps, which allows the Si isotopic analysis of anion-rich solutions, including thermal springs and river waters. In the first step, 2 ml of the sample to be analyzed, containing at least 8 mg.l^{-1} of dissolved Si, are percolated through 2 ml of anion-exchange resin (Biorad AG MP-1) in order to remove SO_4^{2-} and Cl^- ions. Prior to purification, the anion-exchange resin is washed in batch with HNO_3 (3 × 5 ml) and milliQ water (3 × 5 ml), cleaned successively with 1 M HNO_3, 3 M HNO_3 and 1 M HNO_3, and rinsed with milli-Q water until a neutral pH is reached (Appendix C). The anion-free solution is then percolated through 1.8 ml of a pre-cleaned cation-exchange resin (Biorad AG50W-X12; Georg et al., 2006) with 4 ml of milli-Q water. The volume of the purified sample for isotopic analysis is 8 ml and the concentration of dissolved Si is ≥2 mg.l^{-1}.

The Si isotope compositions of 9 thermal springs (RM2, CC, CE, GC, GA, GAB, TA, Sofaïa, BCM), 15 river waters (rNogent, rMoustique Ste-Rose, rPP, rGP, rRR, rCorossol, rBD, rQC, rPBD, rCap, rRC, rCC, rRouge, rGC, rGAam), 7 soil solutions (GBD2) and the hydrothermally-altered rock from Les Mamelles were determined after sample treatment using the two-step purification method. The hydrothermally-altered rock was first digested by alkaline fusion with NaOH (Georg et al., 2006) prior to purification; the Na concentration in the resulting solution was below the detection limit (< 0.43 µmol.l^{-1}). The SO_4^{2-} and Cl^- concentrations in all the purified solutions were < 1.5 and < 3.1 µmol.l^{-1}, respectively, i.e. below the detection limits for these anions. The Si recovery in all the solutions was always >98% and the blank level was below the ICP-OES detection limit for Si (i.e. < 0.36 µmol.l^{-1}).

3.4.2. Mass spectrometry

The Si isotope composition of the thermal spring, river water, soil solution and hydrothermally-altered rock samples were determined by MC-ICP-MS (Neptune Plus™ High Resolution Multicollector ICP-MS, Thermo Fisher Scientific) in wet plasma mode and medium resolution (Δm/m ~ 6000), using a PFA nebulizer of 100 µl.min^{-1} uptake rate. The instrumental mass bias was corrected using the standard-sample bracketing technique and an external Mg doping (Cardinal et al., 2003). The analyses were performed in a 2% *v*/v HNO_3 matrix, with a typical sensitivity of 7 V for 2 mg.l^{-1} Si and an instrumental blank <30 mV. Silicon isotope compositions are expressed in relative deviations of $^{30}Si/^{28}Si$ ratio from the NBS-28 reference standard using the common δ-notation (‰): $\delta^{30}Si = [(^{30}Si/^{28}Si)_{sample}/(^{30}Si/^{28}Si)_{NBS\text{-}28} - 1] \times 1000$. One measurement comprises 30 cycles with 4.2 s integration time corrected by blank in a 2% v/v HNO_3 matrix. Each single δ-value represents one sample run and two bracketing standards. $\delta^{30}Si$-values are reported as the mean of replicate isotopic analyses ± SD. When $n = 1$, SD is the standard deviation of the two $\delta^{30}Si$ obtained for a sample relative to the two bracketing standards. When $n > 1$, SD is the pooled deviation standard corresponding to $[(SD_1^2 + SD_2^2 + \ldots + SD_n{}^n)/n]^{0.5}$. If SD < 0.005, the SD value reported is 0.01. Quality control of mass bias was performed by ensuring that $\delta^{30}Si$ and $\delta^{29}Si$ measurements fit to a mass-dependent fractionation array, supporting the interference-free determination of all three Si isotopes via MC-ICP-MS (Appendix D).

3.4.3. Precision and accuracy

The long-term precision and accuracy of the MC-ICP-MS $\delta^{30}Si$ analyses were assessed from multiple measurements of three reference materials prepared using the single step cation-exchange resin method after alkaline fusion with NaOH (Georg et al., 2006). These checks were performed within each analytical session over a period of nine months. The values obtained for diatomite ($\delta^{30}Si = 1.29 \pm 0.09$‰, SD, $n = 19$), USGS basalt BHVO-2 ($\delta^{30}Si = -0.27 \pm 0.06$‰, SD, $n = 10$) and quartz Merck ($\delta^{30}Si$ of 0.04 ± 0.09‰, SD, $n = 6$) (Fig. 3; Appendix E) are consistent with those reported earlier (Reynolds et al., 2007; Abraham et al., 2008).

The absence of Si isotope fractionation during the two-step purification method was verified by running the solutions obtained after digestion by alkaline fusion of the diatomite, BHVO-2 and quartz Merck reference materials. One set of diatomite and BHVO-2 solutions was spiked with SO_4^{2-} and Cl^- to mimic an anion-rich matrix containing 100 and 400 mg SO_4^{2-}.l^{-1} and 50 and 100 mg Cl^-.l^{-1} (Appendix E). The reproducibility of the two-step purification method was assessed by performing replicate measurements of the reference materials. The replicates are either full replicates, i.e. each measurement corresponds to the reference material subjected to digestion by alkaline fusion and two-step purification (noted as F in Appendix E), or to partial replicates, i.e. each measurement corresponds to the same sample of reference material obtained after alkaline fusion but the two-step purification method was repeated (noted as C in Appendix E). The Si isotope compositions of diatomite ($\delta^{30}Si$ of 1.34 ± 0.07‰, $n = 7$), BHVO-2 ($\delta^{30}Si$ of −0.37 ± 0.07‰, $n = 3$) and quartz Merck ($\delta^{30}Si$ of 0.04 ± 0.05‰, $n = 9$) subjected to the newly-developed two-step purification method are in good agreement with those obtained using the single step cation-exchange resin. The results also match previously published values (Fig. 3; Appendix E).

4. Results

4.1. Major element compositions

The chemical compositions of the thermal spring, river water and soil solution samples are presented in Table 1.

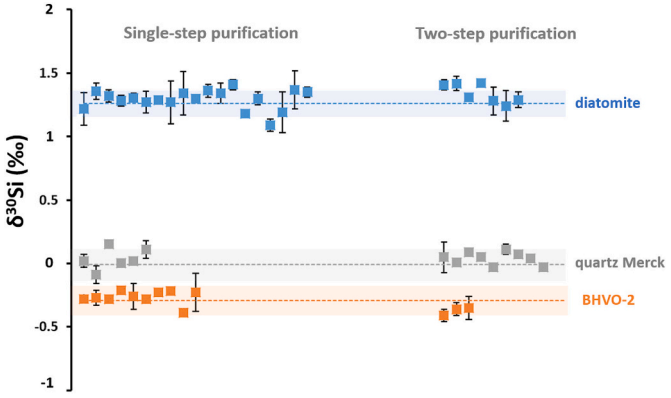

Fig. 3. Plot of the $\delta^{30}Si$ values (± SD) of the three reference materials (diatomite, quartz Merck and BHVO-2) as obtained using a single purification (cation-exchange resin) and the two-step purification method (cation-exchange resin + anion-exchange resin) developed in this study. The data are reported in Appendix E. Our $\delta^{30}Si$ values agree well (within error) with the Si isotope compositions (dashed line ± SD shown as a colored box) reported for the diatomite, quartz Merck and BHVO-2 reference materials (Reynolds et al., 2007; Abraham et al., 2008).

4.1.1. Thermal springs

The spring BCM has the highest temperature (~58 °C), whereas RM2 and CE correspond to cold spring waters (~21 °C), in accordance with Brombach et al. (2000) and Villemant et al. (2005, 2014). Except Dolé (pH 8.3), all the thermal discharges are slightly (pH 6.3–6.7; CC, GC, HR), moderately (pH 4.5–5.9; RM3, CE, GA, GAB, GAF, BJ, PR, TA, BM) and strongly (pH 3.3–3.8; RM2, Sofaïa) acidic. In accordance with previous studies (Brombach et al., 2000; Villemant et al., 2005; Villemant et al., 2014; Dessert et al., 2015), the thermal springs are classified in three groups based on their major anion (SO_4^{2-}, Cl^- and HCO_3^-) and cation (Ca, Mg and Na) contents (Fig. 4): Ca-SO_4 waters (RM2, RM3, CE, GA, GAB, GAF, BJ, PR, TA, Sofaïa, BCM), Ca-Na-Cl waters (GC, CC) and Ca-Na-HCO_3 waters (Dolé, HR).

The Ca-SO_4 thermal springs are acidic (pH: 3.3–5.9) and except BCM and Sofaïa, they are all located in the Amic crater (Fig. 1). They exhibit SO_4^{2-} and Cl^- concentrations ranging from 358 (Sofaïa) to 8752 μmol.l^{-1} (CE) μmol.l^{-1} and from 301 (CE) to 7930 (GA) μmol.l^{-1}, respectively. According to Brombach et al. (2000), the acidity and SO_4^{2-} content of these springs originate from the oxidation of hydrogen sulfide at shallow levels in the hydrothermal system. The presence of Cl^- in significant concentrations in GA, GAB, GAF is due to mixing with neutral pH and Cl-rich waters. The Ca-Na-Cl thermal springs are slightly acidic (pH: 6.3–6.7) and are located on the eastern side of the Amic crater (Fig. 1). They exhibit Ca and Na concentrations ranging from 1608 (CC) to 2801 μmol.l^{-1} (GC) and from 2636 (CC) to 4047 (GC) μmol.l^{-1}, respectively. The Ca-Na-HCO_3 thermal springs display near-neutral to alkaline pH values (6.5–8.3) and are located outside the Amic crater (Fig. 1). Sodium is their major cation, with concentrations ranging from 1020 (HR) to 1690 μmol.l^{-1} (Dolé) μmol.l^{-1}, followed by Ca (484–1293 μmol.l^{-1}).

4.1.2. River waters

Sulfate and Cl^- are the major anions in the river waters. The concentrations range from 95 (rPP) to 3403 (rGAav) μmol.l^{-1} and from 132 (rRouge) to 5643 (rGC) μmol.l^{-1}, respectively. Following Gaillardet et al. (2011), we assume that rivers with a Cl^-/SO_4^{2-} molar ratio < 8–10 and a SO_4^{2-} concentration > 25–50 μmol.mol^{-1} are impacted by hydrothermal activity. The river compositions were first corrected for atmospheric salt contribution using Cl^- as a conservative element. The concentration of atmospheric Cl^- in rivers is obtained by multiplying the Cl^- concentration in rainfall (92 μmol.l^{-1}; Dessert, unpublished data) by the evapotranspiration factor (~1.5; Lloret et al., 2011). According to this calculation, the concentration of atmosphere-derived Cl^- in the rivers is 138 μmol.l^{-1}. This estimate is in good agreement with the Cl^- concentration of rRouge (140 μmol.l^{-1}; Table 1) which is believed to derive solely from atmospheric inputs (Dessert et al., 2015).

Table 1 indicates that thirteen (rPP, rGP, rRR, rRM, rRC, rCC, rCE, rRN, rRouge, rGC, rGAam, rGAav, rGAb) out of the 22 rivers collected on Basse-Terre display a molar Cl^-/SO_4^{2-} ratio < 8–10 and a SO_4^{2-} concentration > 25–50 μmol.mol^{-1}, likely pointing to hydrothermal inputs (Fig. 5). These rivers will be referred in the following sections as "HI" rivers. The river waters displaying a molar Cl^-/SO_4^{2-} ratio > 8–10 and/or a SO_4^{2-} < 25–50 μmol.mol^{-1} (rNogent, rMoustique Ste-Rose, rCorossol, rBD, rQC, rCAE, rPBD, rCap, rSaint-Louis) and which presumably are not influenced by hydrothermal contributions will be called NI rivers.

The temperature (18.8–31.5 °C) and pH (4.0–7.6) values of the HI rivers compare with the values measured for the NI rivers (21.7–25.7 °C and 4.8–8.2, respectively). However, conductivity (and hence the

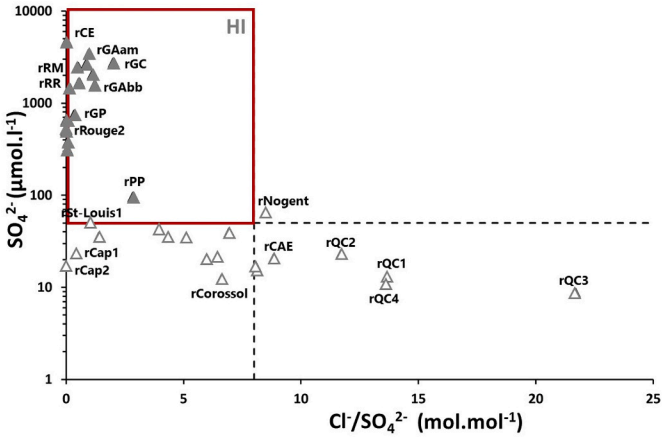

Fig. 5. Plot showing the SO_4^{2-} concentration (μmol.l^{-1}) as a function of the Cl^-/SO_4^{2-} molar ratio measured in the river water samples. Following Gaillardet et al. (2011), the river compositions which fall in the red-framed area of the graph (SO_4^{2-} > 25–50 μmol.l^{-1} and Cl^-/SO_4^{2-} < 8–10) are affected by volcanic hydrothermal inputs; these river waters are denoted by "HI". The hydrothermally-impacted rivers (plain grey triangle) are distinguished from the non-impacted rivers (open grey triangle). Sample codes as in Table 1. (Single column fitting image). (For interpretation of the references to colour in this figure legend, the reader is referred to the web version of this article.)

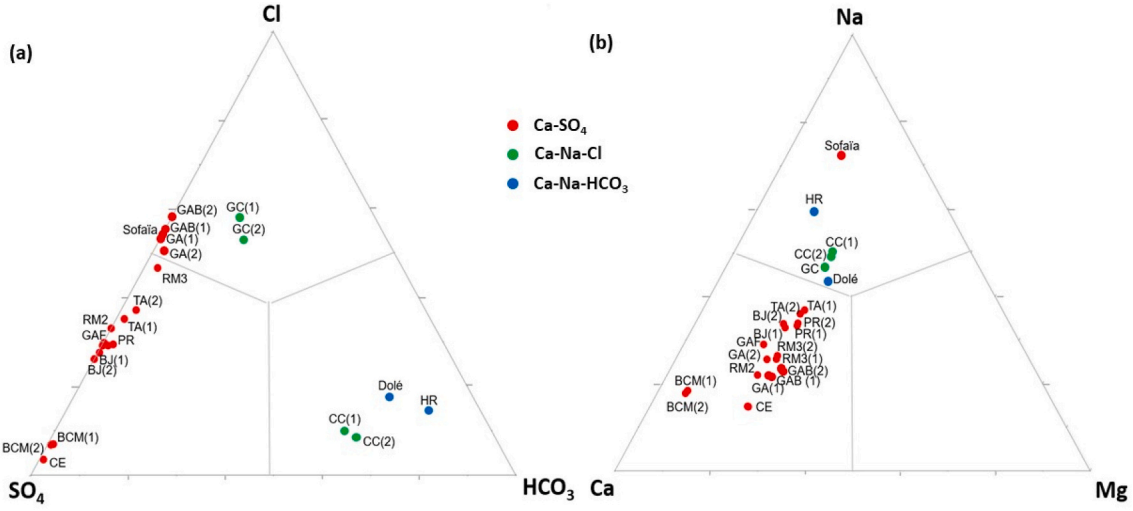

Fig. 4. Ternary diagrams of the major anion (a) and cation (b) composition of the thermal springs studied. The HCO_3 concentration is calculated based on the measured alkalinity and the charge balance. The samples are grouped as Ca-SO_4 (red), Ca-Na-Cl (green) and Ca-Na-HCO_3 (blue) waters. (2 column fitting image.) (For interpretation of the references to colour in this figure legend, the reader is referred to the web version of this article.)

dissolved solid load) are three to six times higher in the HI samples than in the NI samples. Among the HI river waters, rRouge, rRM and rGAam, rGAav, rGAbb display the lowest pH values (pH: 4.0–4.8), whereas rPP and rGP are slightly alkaline (pH: 7.5). The pH of rQC fluctuates (pH: 4.8–5.6) depending on the time of sampling, an observation already made in previous studies (Clergue et al., 2015; Fries et al., 2019). The alkalinity of the NI rivers ranges from 43 (rQC3) to 690 (rSt-Louis) μmol.l^{-1}. The riverine concentration of dissolved Si varies between 444 (rRC) and 1947 (rGAav) μmol.l^{-1}. Our results are in generally good agreement with the river compositions reported by other authors (Rad et al., 2007; Gaillardet et al., 2011; Lloret et al., 2011; Rivé et al., 2013; Clergue et al., 2015; Dessert et al., 2015).

4.1.3. Soil solutions

The Ferralsol soil solutions are acidic (pH: 4.9–5.5). Sulfate and Cl^- concentrations are in the ranges 13–20 and 217–278 μmol.l^{-1}, respectively. Sodium (170–241 μmol.l^{-1}) is the major cation for all soil depths. The concentration of dissolved Si varies between 63 (at a depth of 152 cm) and 116 (at a depth of 457 cm) μmol.l^{-1}. Clergue et al. (2015) and Fries et al. (2019) have reported similar soil solution compositions at Quiock Creek.

4.2. Ge/Si ratios and Si isotope compositions

The Ge/Si ratio values and Si isotope compositions of the thermal spring, river water, soil solution and hydrothermally-altered rock samples are compiled in Table 2 and also plotted in Fig. 6.

4.2.1. Thermal springs

As shown in Fig. 6a, the Ge/Si ratio of the thermal springs of Basse-Terre Island spans a large range of values (0.05–21.03 μmol.mol^{-1}). The two BCM spring samples display the highest ratios. High Ge/Si ratios are also measured in Galion's thermal waters (GA, Ge/Si = 8.33 and 8.86 μmol.mol^{-1} and GAB, Ge/Si = 9.49 and 6.69 μmol.mol^{-1}) and in HR (11.28 μmol.mol^{-1}). All the other springs have much lower Ge/Si ratios, i.e. ≤ 2.30 μmol.mol^{-1} (average 0.97 ± 0.61 μmol.mol^{-1}). The $\delta^{30}Si$ values of the thermal springs range from 0.71 ± 0.05‰ (Sofaïa) to 1.50 ± 0.13‰ (GAB in 2017) (Fig. 6b). The RM2 spring collected in October 2017 and February 2015 display similar Si isotope compositions (1.07 ± 0.08‰ and 1.04 ± 0.02‰, respectively). In contrast, GAB has a lighter Si isotope value in January 2015 (1.06 ± 0.05‰) compared to November 2017 (1.50 ± 0.13‰).

4.2.2. River waters

Thirty out of the 36 riverine samples analyzed display Ge/Si values ~ ≤ 1.1 μmol.mol^{-1} (Fig. 6a). This comprises nine HI rivers (rPP, rGP, rRR, rRM, rRC, rCC, rRN, rRouge and rGC), with the lowest values for rPP and rGP (Table 2), on par with the values measured for the NI rivers (except rQC). Higher Ge/Si ratios are measured in rQC (2017 sample; 1.56–2.57 μmol.mol^{-1}), rCE (1.48 μmol.mol^{-1}), rGAam (3.88 μmol.mol^{-1}), rGAav (5.25 μmol.mol^{-1}) and rGAbb (1.06 μmol.mol^{-1}).

Except rQC, these rivers with higher Ge/Si ratios receive hydrothermal inputs (Fig. 5). The Ge/Si ratio of rPP, rGP and rRR, which drain the extinct hydrothermal system of Les Mamelles, varies in the range 0.19–0.39 μmol.mol^{-1}. The Ge/Si ratio of rRouge, which drains the extinct hydrothermal system of Carmichaël, shows little fluctuations (0.39–0.43 μmol.mol^{-1}) between January 2015, October 2016 and January 2017. In contrast, rQC collected in February 2015 has a lower Ge/Si ratio (0.96 μmol.mol^{-1}) than the samples collected in October and November 2017 (1.56–2.57 μmol.mol^{-1}).

The $\delta^{30}Si$ values of the HI river waters tend to be heavier (1.12–1.54‰) than those measured for the NI river waters (0.26–1.21‰; Fig. 6b). The lowest $\delta^{30}Si$ values correspond to the NI rivers rQC (0.26 ± 0.05‰) and rBD (0.33 ± 0.01‰). Except these two samples, the Si isotope compositions of the rivers do not differ markedly from those of the thermal springs.

4.2.3. Soil water

The Ge/Si ratio of the soil solutions varies between 1.82 and 7.46 μmol.mol^{-1}, but no trend with depth in the soil profile can be inferred (Fig. 6a; Table 2). The highest value (7.46 μmol.mol^{-1}) corresponds to a soil depth of 274 cm. The Si isotope composition of the soil solutions varies between −0.38 ± 0.05‰ (at a depth of 427 cm) and − 1.09 ± 0.04‰ (at a depth of 61 cm) (Fig. 6b).

4.2.4. Hydrothermally-altered rock

The bulk Ge/Si ratio and $\delta^{30}Si$ of the hydrothermally-altered rock are 0.68 μmol.mol^{-1} and -0.35 ± 0.02‰, respectively (Fig. 6a and b). Compared to andesite, the hydrothermally-altered rock has lower Ge/Si (USGS standard AGV-2: 1.59 ± 0.19 μmol.mol^{-1}; Si from the USGS certificate of analysis Wilson, 1998; Ge from Delvigne et al., 2018) and $\delta^{30}Si$ (andesite from Guadeloupe: −0.23 ± 0.05‰; Opfergelt et al., 2012a) values.

5. Discussion

5.1. Ge/Si ratio and Si isotope composition of the thermal springs

The Ge/Si ratio in the thermal spring waters do not reflect their compositional type. For example, the Ge/Si ratio values of the Ca-SO_4 waters and Ca-Na-HCO_3 waters overlap (0.05–21.03 and 0.39–11.28 μmol.mol^{-1}, respectively; Appendix F). The Ge/Si ratios in the Ca-Na-Cl springs also compare with those found for several Ca-SO_4 springs (Table 2; Appendix F).

We note that the two Ca-SO_4 springs (GA and GAB) sampled in 2015 and 2017 exhibit consistently high Ge/Si ratio values (6.69–9.49 μmol.mol^{-1}). Many factors can influence the Si and Ge contents of thermal discharges. The composition of the primary rock reacting with the hydrothermal fluid is one of them, but other processes may control the Ge/Si ratio in solution. In an experimental study, Pokrosvky and Schott (Pokrovsky and Schott, 1998) determined the thermodynamic properties of aqueous Ge(IV) hydroxide complexes from 25 to 350 °C and predicted a strong dependence of the Ge/Si ratio on temperature in aqueous solutions in equilibrium with Ge-bearing silicates. Evans and Derry (2002) investigated Himalayan hot springs and concluded that the wide range of Ge/Si ratios resulted from the progressive precipitation of Ge-poor quartz. These authors also highlighted that mixing of hydrothermal fluids with surface waters influence the Ge/Si ratio in the thermal discharges. Arnórsson (Arnòrsson, 1987) indicates that the Ge/Si ratio in silica sinters from Iceland and New Zealand is always lower than in the thermal waters from which the deposits originate, pointing again to the non-conservative behavior of Ge during silica precipitation. In contrast, the formation of sulfide minerals, such as pyrite, in the hydrothermal system incorporates Ge, producing lower Ge/Si ratios in the liquid phase (Bernstein, 1985). The rate of dissolution and the abundance of hydrothermal alteration minerals that can take up Ge to a variable extent will also govern the relative proportions of Ge and Si in thermal springs. Finally, in shallow hydrothermal systems associated with active volcanoes, high-temperature magmatic gases may contribute Ge and Si to the thermal waters sampled at the surface (de Hoog et al., 2005; Rouxel and Luais, 2017). The broad range of Ge/Si ratio values measured in the thermal springs from Basse-Terre likely results from various and complex interactions, some being more significant than others, perhaps depending on the extent of water-rock interaction prior to resurgence at the surface. A full understanding of the thermal spring's geochemistry requires additional data, including stable isotope measurements, and is out of the scope of this study.

The thermal springs' Si isotope compositions (0.7–1.5‰, Fig. 6b) compare well with the range of values reported for thermal springs worldwide, i.e. -0.6-1.7‰ (Douthitt, 1982; Opfergelt et al., 2011; Geilert et al., 2015; Ding et al., 2017; Chen et al., 2020). Similar to the Ge/Si ratio, the $\delta^{30}Si$ values do not discriminate different spring types (Fig. 6b; Appendix F). Geilert et al. (2015) report the $\delta^{30}Si$ of dissolved Si and

Table 2
Concentration of Ge, Ge/Si ratio, and Si isotope compositions ($\delta^{29}Si$ and $\delta^{30}Si$) of the thermal springs, river waters, soil solutions and hydrothermally-altered rock sampled at Basse-Terre. Eleven springs and seven rivers were collected several times on different dates between 2015 and 2018. The thermal springs are sorted by type, following Brombach et al. (2000)'s classification (see text). Rivers affected by hydrothermal inputs are denoted by "HI".

Label	Type	Ge	Ge/Si	SD	n	$\delta^{29}Si$	SD	$\delta^{30}Si$	SD	n
		nmol.l^{-1}	µmol.mol^{-1}			‰		‰		
Thermal springs										
RM2(1)	Ca-SO_4 water	1.85	1.35	–	1	0.54	0.04	1.04	0.02	2
RM2(2)	Ca-SO_4 water	1.51	1.05	–	1	0.57	0.02	1.07	0.08	1
RM3(1)	Ca-SO_4 water	3.15	1.22	–	1	–	–	–	–	–
RM3 (2)	Ca-SO_4 water	3.60	1.25	–	1	–	–	–	–	–
CE(1)	Ca-SO_4 water	2.34	1.36	–	1	–	–	–	–	–
CE(2)	Ca-SO_4 water	2.62	1.50	–	1	0.63	0.01	1.35	0.05	1
GA(1)	Ca-SO_4 water	25.55	8.86	–	1	0.49	0.02	1.00	0.02	2
GA(2)	Ca-SO_4 water	22.15	8.33	–	1	–	–	–	–	–
GAB(1)	Ca-SO_4 water	27.35	9.49	0.96	14	0.5	0.02	1.06	0.05	1
GAB(2)	Ca-SO_4 water	18.13	6.69	–	1	0.77	0.07	1.50	0.13	3
GAF	Ca-SO_4 water	0.08	0.05	–	1	–	–	–	–	–
BJ(1)	Ca-SO_4 water	0.48	0.26	–	1	–	–	–	–	–
BJ(2)	Ca-SO_4 water	0.69	0.38	–	1	–	–	–	–	–
PR(1)	Ca-SO_4 water	0.91	0.44	–	1	–	–	–	–	–
PR(2)	Ca-SO_4 water	1.25	0.60	–	1	–	–	–	–	–
TA(1)	Ca-SO_4 water	5.00	2.10	–	1	0.67	0.08	1.28	0.12	2
TA(2)	Ca-SO_4 water	5.81	2.30	–	1	–	–	–	–	–
Sofaïa	Ca-SO_4 water	0.53	0.94	–	1	0.37	0.04	0.71	0.05	1
BCM(1)	Ca-SO_4 water	11.72	21.03	–	1	0.64	0.01	1.14	0.02	1
BCM(2)	Ca-SO_4 water	10.67	18.92	–	1	–	–	–	–	–
CC(1)	Ca-Na-Cl water	1.89	1.13	–	1	0.65	0.04	1.22	0.07	2
CC(2)	Ca-Na-Cl water	1.80	1.09	–	1	0.48	0.02	0.99	0.03	1
GC(1)	Ca-Na-Cl water	0.78	0.50	–	1	–	–	–	–	–
GC(2)	Ca-Na-Cl water	0.83	0.56	–	1	0.57	0.01	1.13	0.01	1
HR	Ca-Na-HCO_3 water	14.44	11.28	–	1	–	–	–	–	–
Dolé	Ca-Na-HCO_3 water	0.55	0.39	–	1	–	–	–	–	–
River waters										
rNogent		0.08	0.15	–	1	0.44	0.04	0.83	0.03	1
rMoustique Ste-Rose		0.09	0.30	–	1	0.25	0.04	0.55	0.13	2
rPP	HI	0.10	0.19	–	1	0.53	0.03	1.17	0.06	4
rGP	HI	0.11	0.20	–	1	0.75	0.01	1.50	0.02	2
rRR	HI	0.22	0.39	–	1	0.72	0.01	1.39	0.09	1
rCorossol		0.14	0.34	–	1	0.51	0.04	0.97	0.03	1
rBD1		0.08	0.19	–	1	–	–	–	–	–
rBD2		0.11	0.28	–	1	–	–	–	–	–
rBD3		0.11	0.30	–	1	–	–	–	–	–
rBD4		0.09	0.24	–	1	0.15	0.01	0.33	0.01	1
rQC1		0.09	0.96	–	1	0.20	0.05	0.47	0.01	1
rQC2		0.11	1.56	–	1	–	–	–	–	–
rQC3		0.14	2.00	–	1	–	–	–	–	–
rQC4		0.19	2.57	–	1	0.09	0.01	0.26	0.05	2
rCAE		0.16	0.42	–	1	–	–	–	–	–
rPBD1		0.06	0.15	–	1	0.53	0.02	0.95	0.04	1
rPBD2		0.11	0.31	–	1	–	–	–	–	–
rPBD3		0.08	0.25	–	1	–	–	–	–	–
rRM	HI	1.39	0.93	0.01	2	–	–	–	–	–
rCap1		0.18	0.42	0.02	2	0.58	0.01	1.21	0.02	1
rCap2		0.14	0.65	–	1	–	–	–	–	–
rRC1	HI	0.39	0.80	–	1	0.59	0.02	1.12	0.08	3
rRC2	HI	0.28	0.62	–	1	–	–	–	–	–
rRC3	HI	0.28	0.62	–	1	–	–	–	–	–
rCC	HI	0.23	0.35	–	1	0.60	0.01	1.15	0.01	1
rCE	HI	0.28	1.48	–	1	–	–	–	–	–
rRN	HI	0.84	0.61	–	1	–	–	–	–	–
rSt-Louis1		0.15	0.28	–	1	–	–	–	–	–
rSt-Louis2		0.14	0.29	–	1	–	–	–	–	–
rRouge1	HI	0.26	0.43	–	1	0.78	0.07	1.47	0.11	3
rRouge2	HI	0.21	0.39	–	1	0.64	0.01	1.28	0.03	1
rRouge3	HI	0.22	0.40	–	1	–	–	–	–	–
rGC	HI	0.54	0.43	–	1	0.70	0.04	1.54	0.07	1
rGAam	HI	6.80	3.88	–	1	0.68	0.01	1.33	0.09	1
rGAav	HI	10.21	5.25	–	1	–	–	–	–	–
rGAbb	HI	1.19	1.06	–	1	–	–	–	–	–
Soil solutions										
GBD2–61		0.25	2.99	–	1	−0.60	0.04	−1.09	0.04	1
GBD2–91		0.25	2.59	–	1	−0.37	0.01	−0.66	0.04	1
GBD2–152		0.28	4.40	–	1	−0.40	0.01	−0.79	0.04	1
GBD2–274		0.52	7.46	–	1	−0.41	0.08	−0.69	0.01	1
GBD2–344		0.17	2.67	–	1	−0.26	0.01	−0.54	0.01	2
GBD2–457		0.22	1.90	–	1	−0.19	0.05	−0.38	0.05	1

(*continued on next page*)

Table 2 (*continued*)

Label	Type	Ge	Ge/Si	SD	n	$\delta^{29}Si$	SD	$\delta^{30}Si$	SD	n
		nmol.l^{-1}	µmol.mol^{-1}			‰		‰		
GBD2–823		0.19	1.82	–	1	−0.29	0.01	−0.52	0.04	1
Hydrothermally altered rock										
		5524.86	0.68	–	1	−0.19	0.04	−0.35	0.02	1

-: not measured.

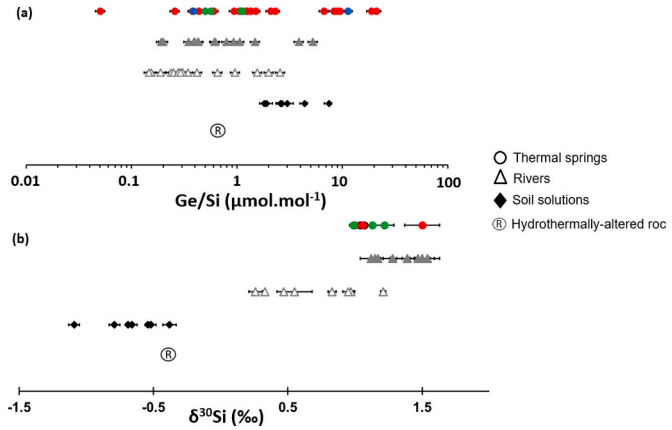

Fig. 6. Plots showing the Ge/Si ratio (± SD) (a) and Si isotope composition ($\delta^{30}Si$ ± SD) (b) of the thermal spring (circle), river water (triangle), soil solution (diamond) and hydrothermally-altered rock (®) samples. The Ca-SO_4, Ca-Na-Cl and Ca-Na-HCO_3 thermal springs are shown with red, green and blue-filled symbols, respectively. The hydrothermally-impacted rivers (plain grey triangle) are distinguished from the non-impacted rivers (open grey triangle). (1.5 column fitting image). (For interpretation of the references to colour in this figure legend, the reader is referred to the web version of this article.)

silica sinter from the Geysir geothermal area, Iceland, and show that the deposit becomes progressively isotopically lighter downstream from the resurgence. While the isotope fractionation correlates inversely with temperature, the authors highlight that the dominant control is the rate at which silica precipitates from the flowing spring waters. A similar observation was made at Yellowstone National Park, USA (Chen et al., 2020). These results corroborate previous experimental observations (Geilert et al., 2014) and isotope modelling (Kleine et al., 2018). Akin weathering reactions in soils (Opfergelt and Delmelle, 2012; Frings et al., 2016), the formation of clay minerals (e.g., kaolinite and smectite) during water-rock interaction in the subsurface hydrothermal system may also fractionate Si isotopes by depleting the source solution in ^{28}Si. The light Si isotope composition of the clayey hydrothermally-altered rock ($\delta^{30}Si = -0.35$‰) supports this idea. Thus, both silica deposition and alteration reactions in different parts of the hydrothermal system(s), extinct and active, are likely responsible for the variations in the Si isotope composition of the thermal springs across Basse-Terre Island.

5.2. Ge/Si ratio and Si isotope compositions of rivers

The Ge/Si ratio in the river samples (0.15–5.25 µmol.mol^{-1}) do not differ significantly from the values measured for the thermal waters, although a few springs (GA, GAB, HR and BCM) are characterized by much higher values (Fig. 5). The riverine Ge/Si ratios are within the range of values reported for other river systems in the world (0.16–20 µmol.mol^{-1}; e.g., Mortlock and Froelich, 1987; Froelich et al., 1992; Derry et al., 2005; Lugolobi et al., 2010; Han et al., 2015; Baronas et al., 2018). They are also in good agreement with the few analyses reported for rivers draining volcanic terrains elsewhere (0.18–3.16 µmol.mol^{-1}; Derry et al., 2005; Baronas et al., 2018; Ameijeiras-Mariño et al., 2018).

Using chemical and Mg isotope compositions, Dessert et al. (2015) showed that the river chemistry on Basse-Terre Island is the result of mixing in various proportions of rainwater, water that has reacted with andesitic rocks, water draining through highly-weathered soils, water leaching extinct hydrothermal areas and thermal water associated with La Soufrière volcano. The authors also emphasize that the contributions of these end-members vary from north to south and from east to west, reflecting the influence of bedrock age and rainfall gradient.

The wet atmospheric contribution to the Ge and Si concentrations in Basse-Terre's river is not known. According to Heartsill-Scalley et al. (2007), the Si concentration in rainwater collected in Puerto Rico, also a subtropical island, is less than 1.1 mg.l^{-1} and does not vary seasonally. The Ge concentration in rainwater can be assumed to be negligible, as suggested by the low Ge concentrations reported in rainwater from Tallahassee, USA (Ge = 1.7–7.3 ng.l-1; Hambrick et al., 1984). A contribution to atmospheric Ge from fly ash (Aguirre et al., 2017) can also be neglected in Guadeloupe. As mentioned above, our river water samples were collected upstream of croplands and we dismiss an indirect influence of Si-accumulating plants on the riverine Ge/Si ratios.

Since the Ge/Si ratio values of the HI rivers (0.19–5.25 µmol.mol^{-1}) largely overlap with those of the NI rivers (0.15–2.57 µmol.mol^{-1}) (Fig. 6a), the Ge/Si ratio cannot be used to trace a potential hydrothermal contribution. The majority of the HI rivers display a heavier Si isotope composition than that measured for the NI rivers. However, the $\delta^{30}Si$ of the former also tend to be higher than the values obtained for the thermal springs (Fig. 6b), already suggesting an additional control on the isotope composition of the riverine Si. In the next sections, we discuss the Ge/Si ratio and Si isotope compositions of the NI and HI rivers taken separately.

5.2.1. NI rivers

Although the Ge/Si ratios of the NI rivers in the north and in the south of the island overlap, the southern river waters exhibit lower values (0.28–0.65 µmol.mol^{-1}) compared to those typical of the magmatic rock that is being weathered (Ge/Si: 1–3 µmol.mol^{-1} for igneous rocks; Bernstein, 1985; DeArgollo and Schilling, 1978). This is consistent with the preferential incorporation of Ge into the solid phase during chemical weathering and associated clay mineral formation (Kurtz et al., 2002; Derry et al., 2005) and potential adsorption of Ge on aluminum oxides (Scribner et al., 2006). As a result, with the advance of weathering, the Ge/Si ratio in the soil solution can evolve towards higher values when the Ge-rich secondary minerals become instable and dissolve progressively, thereby producing a broad range of compositions (Kurtz et al., 2002). This probably explains the comparatively more variable Ge/Si ratio found for the NI rivers in North Basse-Terre (0.15–2.57 µmol.mol^{-1}; Fig. 7b) as these drain highly weathered terranes dominated by the presence of Vertisols and Ferralsols (Fig. 1).

Similarly, the formation of clay minerals during chemical weathering typically depletes the soil solution in ^{28}Si, leaving behind heavier dissolved Si (Ziegler et al., 2005; Opfergelt and Delmelle, 2012). In agreement with this view, rCap (1.21 ± 0.02‰), which drain Andosols in South Basse-Terre, display higher $\delta^{30}Si$ values than rNogent (0.83 ± 0.03‰) and rMoustique Ste-Rose (0.55 ± 0.13‰), which both flow through older terrains in North Basse-Terre. According to Dessert et al. (2015), the Ca/Mg ratio in Basse-Terre's rivers decreases with increasing chemical weathering, i.e. along a south to north age gradient. Fig. 7 shows that the NI rivers (except rQC which drains highly weathered soils) exhibit a large range of Ca/Mg values, but the ratio in the

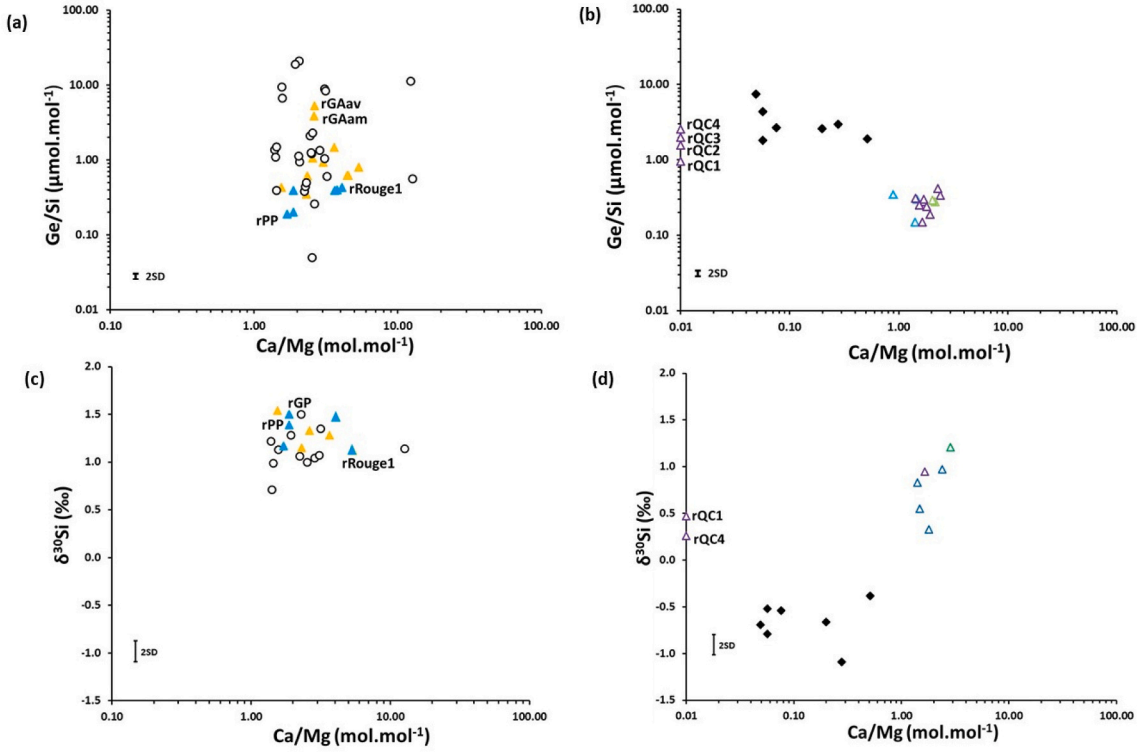

Fig. 7. Plots showing the Ge/Si ratio (a, b) and the Si isotope composition (δ^{30}Si) (c, d) as a function of the Ca/Mg molar ratio in the thermal spring (circle), river water (triangle) and soil solution (diamond) samples. The HI rivers (a, c) that receive discharges from thermal springs (plain orange triangle) are distinguished from those receiving drainages from an extinct hydrothermal system (plain blue triangle). The NI rivers (b, d) are displayed according to their locations in Basse-Terre Island: north (open blue triangle), center (open purple triangle), and south (open green triangle). The 2SD error bar reported correspond to ±10% for Ge/Si, and to the largest 2SD value measured on a sample for δ^{30}Si (Table 2). The river codes are explained in Table 1. (2 column fitting image). (For interpretation of the references to colour in this figure legend, the reader is referred to the web version of this article.)

southern rivers draining less-weathered soils (associated with higher Ge/Si and δ^{30}Si compositions) is higher than in the northern rivers draining more weathered soils (associated with lower Ge/Si ratios and δ^{30}Si compositions).

In contrast to the NI rivers characterized by Ge/Si ratio values <1 µmol.mol^{-1}, the rQC samples display Ge/Si ratio close to or > 1 µmol.mol^{-1} (Table 2). The Quiock creek catchment is underlain by Pleistocene andesitic pyroclasts covered by >15 m of a deeply weathered and cation-depleted regolith (Buss et al., 2010). Clergue et al. (2015) consider that the Li isotope composition of Quiock Creek's drainage waters represents an endmember of such weathering conditions. The regolith contains ~95 wt% of secondary minerals, of which ~65% are halloysite and kaolinite, ~20% are Fe-(oxy)hydroxides and ~ 10% are Al-(oxy)hydroxides (Buss et al., 2010). Accordingly, the soil solution of the Ferralsol from Quiock creek is acidic (pH: 4.2–5.5). It also exhibits a high Ge/Si ratio, i.e. 1.82–7.46 µmol.mol^{-1} (Table 2). Kurtz et al. (2002) found that strongly desilicated (weathered) volcanic soils in Hawaii exhibit high Ge/Si ratios, ranging from 6 to 20 µmol.mol^{-1}. The Ge enrichment of the Hawaiian soils results from preferential fractionation of Ge into the solid phase as clay minerals precipitate out of the soil solution (Kurtz et al., 2002). Moreover, it has been suggested that Al-(oxy)hydroxides may favor Ge adsorption over Si, but the mechanism remains uncertain (Scribner et al., 2006). Derry et al. (2005) explain the high Ge/Si ratios (2–14 µmol.mol^{-1}) measured in the soil solutions from the same strongly weathered volcanic soils in Hawaii by the dissolution of Ge-enriched secondary minerals. Thus, the high Ge/Si ratios measured in our Ferralsol soil solutions likely reflect the dissolution of Ge-rich secondary minerals. We attribute the Ge/Si ratio > 1 µmol.mol^{-1} of rQC as a result of the dissolution under acidic conditions of Ge-rich secondary minerals that accumulated in the Ferralsols due to intense weathering.

The δ^{30}Si compositions of the rQC samples, which represent the most depleted values measured in any of the rivers (Fig. 7c-d, Table 2), support the idea that clay mineral dissolution exerts a major control on the riverine Ge/Si ratio. Since weathering of primary minerals enriches the neoformed clay minerals in ^{28}Si (Ziegler et al., 2005; Opfergelt and Delmelle, 2012), soils that are strongly weathered, and for which the primary mineral reservoir is exhausted, tend to display low δ^{30}Si values (Bern et al., 2010; Opfergelt et al., 2010, 2012a; Baronas et al., 2020). With the advance of weathering under increasingly acidic conditions, the clay minerals are no longer stable and their dissolution releases isotopically light Si in solution.

We further propose that a similar dissolution process partly influences the Si isotope composition of some of the rivers draining the old lithologies of northern Basse-Terre. A candidate is rMoustique Ste-Rose, which based on Mg isotopes, is considered to receive a contribution from the dissolution of ^{26}Mg-rich secondary minerals. As shown by Dessert et al. (2015), the δ^{26}Mg isotope composition of rMoustique Ste-Rose (−0.09‰) is heavier than that of andesitic rocks, whereas other rivers are isotopically lighter. However, we advocate caution in using δ^{26}Mg alone as a proxy for weathering degree since Mg release from secondary minerals in highly weathered soils may be controlled largely by ion exchange reactions rather than by dissolution of Mg-containing secondary minerals (Teng et al., 2010; Huang et al., 2012; Opfergelt et al., 2012b, 2014; Trostle et al., 2014). The rMoustique Ste-Rose displays a light δ^{30}Si (0.55‰) potentially reflecting the isotopically light Si composition from secondary minerals. However, the Ge/Si ratio of this river is low (0.30 µmol.mol^{-1}), i.e. it does not reflect the high Ge/Si from the dissolution of Ge-enriched secondary minerals. This suggests that in the strongly weathered catchment of northern Basse-Terre, riverine Si fluxes involve a contribution from the dissolution of aeolian continental dust (Dessert et al., 2020; Fries et al., 2019), a material characterized by

low $\delta^{30}Si$ (−0.5‰; Ziegler et al., 2005) and Ge/Si ratio (0.5–1 μmol.mol^{-1}; Kurtz et al., 2002) values. Aeolian continental dust in the Caribbean Islands originates from the Sahel and the Sahara (Petit et al., 2005) and is dominated by quartz and mica (Muhs et al., 2010). African dust is mainly deposited by rains, and the catchment of rMoustique Ste-Rose receives ~30% higher mean annual rainfall than the other catchments of northern Basse-Terre (Lloret et al., 2011). This lends credence to the idea that dissolution of aeolian continental dust contributes the Si flux in this river.

5.2.2. HI rivers

Most of the HI rivers are located in southern Basse-Terre and flow through relatively young lithologies (except rPP, rGP and rRR). Some HI rivers from southern Basse-Terre are characterized by Ge/Si values (rCC, rRouge, rGC: 0.35 to 0.43 μmol.mol^{-1}) in the same range than the value measured for rRR in Central Basse-Terre (0.39 μmol.mol^{-1}). Therefore, unlike the NI rivers, the disparity in the Ge/Si ratio values is unlikely to be imparted by different soil weathering degrees. We surmise that the SO_4-rich hydrothermal inputs to the HI rivers have a distinct Ge/Si composition. This is suggested based on a plot of Ge/Si vs. Cl^-/SO_4^{2-} (Fig. 8a). The highest Ge/Si ratio values in some HI rivers from southern Basse-Terre (rGAam, rGAav, rGAbb and rCE) probably reflect the admixing of Ca-SO_4 thermal waters with high Ge/Si ratios, as supported by the higher SO_4^{2-} concentration in these HI rivers (Appendix G). For example, River Galion drains terrains where the thermal discharges are characterized by Ge/Si values >6 μmol.mol^{-1} (i.e. GA and GAB thermal springs: 6.69–9.49 μmol.mol^{-1}, Table 2), low pH and elevated SO_4^{2-} concentrations (Table 1). Similarly, River Carbet collects Ca-SO_4 waters with relatively elevated Ge/Si ratios; the CE thermal spring (Ge/Si ratio: 1.36–1.50 μmol.mol^{-1}, Table 2) being representative of such inputs. Lower Ge/Si values in some HI rivers from southern Basse-Terre (rRM, rRC, rCC, rRN and rGC) likely reflect contributions from thermal waters that are less enriched in Ge compared to hydrothermal discharges affecting River Galion and River Carbet. For example, rCC and rGC receive discharges from Ca-Na-Cl thermal springs, which exhibit relatively low Ge/Si ratios (CC and GC: 0.50–1.13 μmol.mol^{-1}, Table 2).

We argue that the lowest Ge/Si ratios in rPP, rGP, rRR and rRouge (0.19, 0.20, 0.39, 0.40 μmol.mol^{-1}, respectively, Table 2) reflect the Ge and Si concentrations acquired by the rivers' tributaries as they drain through extinct hydrothermal systems, i.e. Les Mamelles for rPP, rGP, rRR, and Carmichaël for rRouge (Fig. 1). The hydrothermally-altered rock collected from the area of Les Mamelles is comprised of pyrophyllite, dickite and pyrite (FeS_2), with minor smectite and residual feldspar (Appendix A). This mineral assemblage is typically encountered when acid-sulfate fluids interact with volcanic rocks in the subsurface hydrothermal system (Reed, 1997). According to Gaillardet et al. (2011), who report field observations of well-developed pyrite veins and hydrothermal weathering features at Les Mamelles, the oxidative dissolution of pyrite in extinct hydrothermal systems provides the source of the high SO_4^{2-} concentration measured in rGP. The oxidative dissolution of pyrite produces sulfuric acid according to the general reaction:

$$4\,FeS_2 + 15\,O_2 + 14\,H_2O \leftrightarrow 8\,H_2SO_4 + 4\,Fe(OH)_3 \quad \text{Eq.1}$$

Our clay-rich, hydrothermally-altered rock specimen has a low Ge/Si value (0.68 μmol.mol^{-1}), which contrasts with the Ge-enrichment usually noticed in secondary clay minerals formed during the meteoric weathering of rocks (Kurtz et al., 2002). The reason for this apparently low accumulation of Ge in the hydrothermal material is not known. Since pyrite tends to incorporate Ge during precipitation from a hydrothermal solution (Bernstein, 1985), its subsequent oxidative dissolution at shallow levels may lead to a progressive loss of Ge in the altered rock, whereas Si would not be modified. Thus, extinct hydrothermal systems such as Les Mamelles release low-pH and SO_4-rich drainages that probably exhibit a low Ge/Si ratio inherited from the dissolution of clayey, hydrothermally-altered rocks found in these areas.

Our riverine $\delta^{30}Si$ measurements suggest that all the NI rivers (0.26–0.97‰) except one are isotopically lighter than the HI rivers (1.12–1.54‰), the NI river rCap1 (1.21‰) being the exception (Table 2). The Si isotope compositions of the HI rivers partly reflect contributions from thermal spring waters with relatively high $\delta^{30}Si$ values (Fig. 8b). However, the high $\delta^{30}Si$ of rCap1 indicates that ^{30}Si-enriched riverine compositions are not necessarily linked to hydrothermalism. As discussed earlier, the isotope composition of dissolved Si in NI rivers is strongly dictated by soil weathering degree; rivers (such as rCap1) which drain younger soils typically display heavier values than rivers flowing through older terrains. Since the HI rivers which receive thermal spring discharges exhibit similar $\delta^{30}Si$ values as those collecting drainages from extinct hydrothermal systems (Fig. 8b), Si isotopes cannot be used to differentiate between the two types of hydrothermal contributions.

6. Conclusions

We carried out an extensive sampling campaign of volcanic thermal springs and river waters in Basse-Terre Island with the objective to gain insight into the influence of hydrothermalism on the riverine Ge/Si ratio and Si isotope compositions, and to assess if the Ge/Si ratio and $\delta^{30}Si$ can act as good indicators of weathering in volcanic terranes featuring both extinct and active hydrothermal manifestations. In order to address these goals, we successfully developed a method allowing the reliable

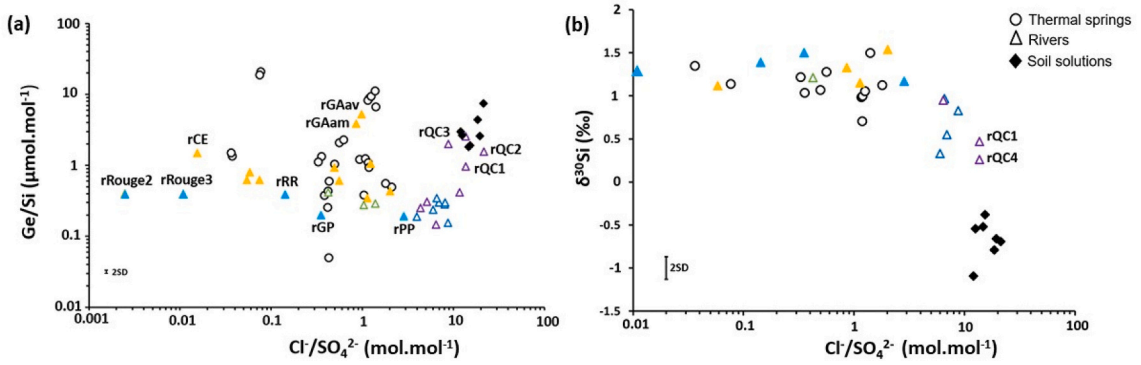

Fig. 8. Plots showing the Ge/Si ratio (a) and the Si isotope composition ($\delta^{30}Si$) (b) as a function of the Cl^-/SO_4^{2-} molar ratio in the thermal spring (circle), river water (triangle) and soil solution (diamond) samples. The HI rivers that receive discharges from thermal springs (plain orange triangle) are distinguished from those receiving drainages from an extinct hydrothermal system (plain blue triangle). The NI rivers are displayed according to their locations in Basse-Terre Island: north (open blue triangle), center (open purple triangle), and south (open green triangle). The 2SD error bar reported correspond to ±10% for Ge/Si, and to the largest 2SD value measured on a sample for $\delta^{30}Si$ (Table 2). The river codes are explained in Table 1. (2 column fitting image). (For interpretation of the references to colour in this figure legend, the reader is referred to the web version of this article.)

determination of Si isotopes in anion (SO_4^{2-} and Cl^-)-rich aqueous solutions. The new method, which involves a two-step purification of the sample using ion exchange resins, expands our capacity to characterize the Si isotope composition of natural waters, such as thermal springs, rivers affected by hydrothermal discharges, river plume waters and seawater, which were hitherto difficult to measure. The following principal conclusions can be drawn using our data:

(i) The thermal springs display a broad range of Ge/Si ratio and $\delta^{30}Si$ values with no apparent relationship to their compositional types. The Ge/Si ratio and Si isotope composition of the thermal springs are probably the result of various processes, including wall-rock alteration and precipitation reactions occurring along the hydrothermal flow paths and at different temperatures.

(ii) The Ge/Si ratio and $\delta^{30}Si$ measured for the NI rivers record different degrees of soil weathering. The rivers which drain the south (younger lithologies) of Basse-Terre display a narrow range of Ge/Si ratios and heavier $\delta^{30}Si$ than the river waters sampled in the north (older lithologies). When the watershed drains highly weathered terrains where the soil mineral reserve has been almost or completely exhausted, dissolution of Ge- and ^{28}Si-rich secondary minerals under acidic conditions enriches the soil solution in Ge and ^{28}Si, thereby increasing and lowering the riverine Ge/Si ratio and $\delta^{30}Si$ values, respectively.

(iii) The Ge/Si ratio imparted to rivers due to weathering is largely concealed when thermal spring discharges mix with river waters. Although the Si isotope composition of such rivers is also affected, the isotopically light signature inherited from highly weathered terranes may still persist.

(iv) Watersheds draining areas where hydrothermal activity took place in the past collect SO_4-rich tributaries that appear to be depleted in Ge relative to Si. We tentatively attribute this characteristic to the leaching and dissolution of clay-rich, hydrothermally-altered rocks, which also display low Ge/Si ratio values. The use of the Cl^-/SO_4^{2-} ratio and SO_4^{2-} concentrations cannot discriminate rivers impacted by contributions from weathering of an extinct hydrothermal system or fluids from an active hydrothermal system. We propose that the determination of the Ge and Si concentrations can circumvent this difficulty.

Overall, our results provide new evidence that Ge/Si ratio and Si isotopes determinations in river waters are powerful tracers of weathering sources. However, in volcanic terranes, they are poor indicators of hydrothermal contributions, except perhaps when these are represented by acid SO_4-rich thermal spring discharges, which seem to exhibit high Ge/Si ratios. When used in combination with the Cl^-/SO_4^{2-} ratio and the SO_4^{2-} concentrations, the Ge/Si ratio can separate rivers impacted by active hydrothermalism from those affected by tributaries draining an extinct hydrothermal system.

Declaration of Competing Interest

The authors declare that they have no known competing financial interests or personal relationships that could have appeared to influence the work reported in this paper.

Acknowledgments

Field work would not have been possible without the professional and enthusiastic support of the INSU-CNRS observatories (Observatoire de l'Eau et de l'Erosion aux Antilles (OBSERA) and Observatoire Volcanologique et Sismologique de Guadeloupe (OVSG)) run by the IPGP. A. Iserentant, C. Givron and H. Dailly (ELI-MOCA, UCLouvain) are warmly thanked for their assistance with the sample analysis. We thank L.A. Derry for access to HR-ICP-MS and for hosting Y.A.M. in the Department of Earth and Atmospheric Sciences, Cornell University. M. Brzezinski kindly shared the diatomite reference material for the Si isotope measurements. The manuscript benefited from discussions with C. Delvigne and C. Hirst. We thank A. Perez-Fodich and one anonymous reviewer for their constructive comments to improve the manuscript. Y. A.M. benefited from an IAGC PhD Student Grant 2015 to carry out Ge analyses at Cornell University. The financial support from the Fund for Scientific Research FNRS in Belgium (grant N°26043653 and FC69480) and from the European Union's Horizon 2020 research and innovation program (grant agreement N°714617) is gratefully acknowledged.

Appendix A

Diffractogram of the hydrothermally-altered rock located on the flanks of Grande Plaine river water obtained by X-ray diffraction (XRD). The hydrothermally-altered rock sample is composed of (1) smectite, (2) pyrophyllite, (3) dickite, (4) feldspar and (5) pyrite

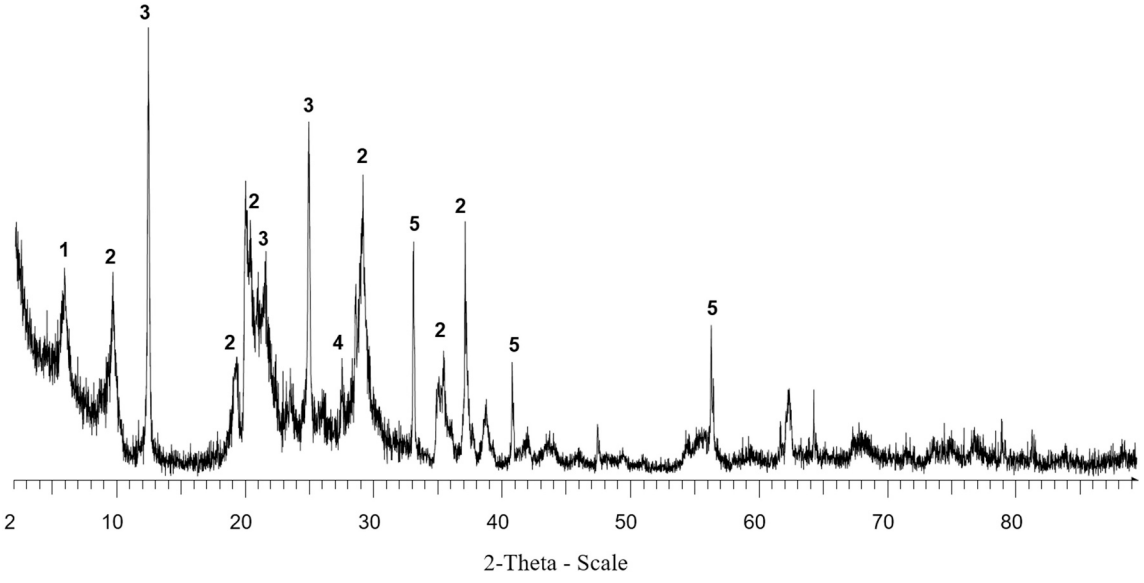

Appendix B

Germanium concentrations measured by HR-ICP-MS (Ge*), Ge concentrations measured by ICP-MS (Ge), and Ge*/Si and Ge/Si ratios calculated using Si concentrations measured by ICP-OES (Table 1) in 12 thermal springs and 17 river waters from Basse-Terre Island

Label	Ge*	Ge*/Si	Ge	Ge/Si
	$nmol.l^{-1}$	$\mu mol.mol^{-1}$	$nmol.l^{-1}$	$\mu mol.mol^{-1}$
Thermal springs				
RM2(1)	1.83	1.33	1.85	1.35
RM3 (2)	3.11	1.21	3.60	1.25
GA(1)	25.25	8.76	25.55	8.86
GAB(1)	27.03	10.53	27.35	9.49
GAF	0.07	0.05	0.08	0.05
PR(1)	0.90	0.43	0.91	0.44
TA(1)	4.94	2.07	5.00	2.10
Sofaïa	0.52	0.92	0.53	0.94
BCM(1)	11.58	20.71	11.72	21.03
CC(1)	1.87	1.11	1.89	1.13
GC(1)	0.76	0.49	0.78	0.50
Dolé	0.53	0.38	0.55	0.39
River waters				
rMoustique Ste-Rose	0.09	0.29	0.09	0.30
rPP	0.10	0.19	0.10	0.19
rCorossol	0.14	0.34	0.14	0.34
rBD1	0.08	0.18	0.08	0.19
rCAE	0.16	0.41	0.16	0.42
rPBD1	0.05	0.14	0.06	0.15
rRM	1.38	0.96	1.39	0.93
rCap1	0.18	0.43	0.18	0.42
rRC1	0.38	0.78	0.39	0.80
rCC	0.22	0.34	0.23	0.35
rRN	0.83	0.68	0.84	0.61
rSt-Louis1	0.15	0.27	0.15	0.28
rRouge1	0.25	0.42	0.26	0.43
rGC	0.53	0.42	0.54	0.43
rGAam	6.72	3.83	6.80	3.88
rGAav	10.10	5.18	10.21	5.25
rGAbb	1.18	1.05	1.19	1.06

Appendix C

Separation scheme through anionic resin (developed in this study) and cationic resin (adapted from Georg et al., 2006) considering the preparation of a water sample with a Si concentration of 8 $mg.l^{-1}$ (minimum). The neutral pH before sample load is checked with a pH paper (pH = 7 ± 0.5)

2 ml resin bed of Biorad AG MP-1		
Separation stage	Solution matrix	Volume (ml)
Pre-cleaning	1 M HNO_3	2
Pre-cleaning	3 M HNO_3	2
Pre-cleaning	1 M HNO_3	2
Pre-cleaning	milli-Q water	10 (pH should be neutral)
Sample load	Acidified water sample	2
Elution	milli-Q water	1
Elution	milli-Q water	1
Result		4 ml at 4 $mg.l^{-1}$ Si
1.8 ml resin bed of Biorad AG 50 W-X12		
Separation stage	Solution matrix	Volume (ml)
Pre-cleaning	3 M HCl	3
Pre-cleaning	6 M HCl	3
Pre-cleaning	concentrated HCl	3

(*continued on next page*)

(*continued*)

2 ml resin bed of Biorad AG MP-1		
Separation stage	Solution matrix	Volume (ml)
Pre-cleaning	6 M HCl	3
Pre-cleaning	3 M HCl	3
Pre-cleaning	milli-Q water	10 (pH should be neutral)
Sample load	Acidified water sample	4
Elution	milli-Q water	2
Elution	milli-Q water	2
Result		8 ml at 2 mg.l^{-1} Si

Appendix D

Plot showing that the δ^{29}Si and δ^{30}Si compositions (± SD) of the thermal spring, river water, soil solution and hydrothermally-altered rock samples fall within error of the mass dependent fractionation array. The slope of the regression line (0.5178) supports an interference-free determination of all three Si isotopes via MC-ICP-MS (Young et al., 2002)

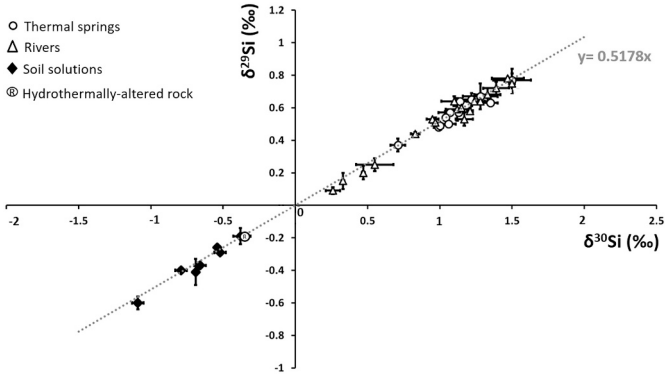

Appendix E

Silicon isotope compositions (δ^{29}Si and δ^{30}Si) of the reference materials diatomite, BHVO-2, and quartz Merck measured after one-step purification, or with the new two-step purification method (An = anion). F1, F2, F3 stand for solutions from separate alkaline fusions. C1, C2, C3, C4, C5, C6 stand for solutions from separate purification onto different columns of exchange resin. The average Si isotope values obtained after one-step or two-step purification are compared with existing Si isotope values reported in the literature for these reference materials

Meas. date[1]	Sample	δ^{29}Si (‰)	SD	δ^{30}Si (‰)	SD	n
14.06.18	DiatomiteF1	0.66	0.10	1.22	0.13	
14.06.18	DiatomiteF1	0.72	0.01	1.36	0.06	
15.06.18	DiatomiteF1	0.62	0.06	1.32	0.05	
10.07.18	DiatomiteF1	0.63	0.02	1.28	0.04	
11.10.18	DiatomiteF1	0.64	0.05	1.31	0.03	
12.10.18	DiatomiteF1	0.66	0.06	1.27	0.09	
12.10.18	DiatomiteF1	0.66	0.03	1.29	0.01	
07.02.19	DiatomiteF3C1	0.74	0.02	1.27	0.17	
07.02.19	DiatomiteF3C1	0.67	0.10	1.34	0.17	
08.02.19	DiatomiteF3C1	0.65	0.02	1.30	0.01	
22.02.19	DiatomiteF3C1	0.63	0.06	1.36	0.05	
22.02.19	DiatomiteF3C1	0.61	0.04	1.34	0.08	
22.02.19	DiatomiteF3C1	0.66	0.05	1.41	0.04	
22.02.19	DiatomiteF3C1	0.79	0.05	1.18	0.03	
04.03.19	DiatomiteF3C1	0.74	0.05	1.30	0.05	
04.03.19	DiatomiteF3C1	0.58	0.01	1.09	0.05	
22.02.19	Diatomite F3C2	0.69	0.07	1.19	0.16	
26.02.19	Diatomite F3C2	0.72	0.06	1.37	0.15	
08.02.19	Diatomite F3C3	0.76	0.02	1.35	0.04	
14.06.18	AnDiatomiteF2C1	0.65	0.08	1.41	0.04	

(*continued on next page*)

(*continued*)

Meas. date[1]	Sample	δ^{29}Si (‰)	SD	δ^{30}Si (‰)	SD	n
15.06.18	AnDiatomiteF2C1	0.68	0.02	1.42	0.06	
08.02.19	AnDiatomiteF3C2	0.69	0.01	1.31	0.02	
08.02.19	AnDiatomiteF3C3	0.60	0.01	1.42	0.03	
22.02.19	AnDiatomiteF3C4 100 50[2]	0.76	0.01	1.28	0.11	
22.02.19	AnDiatomiteF3C5 400 300[2]	0.67	0.10	1.24	0.12	
22.02.19	AnDiatomiteF3C6	0.57	0.06	1.29	0.06	
	Average diatomite (one-step purification)	**0.67**	**0.06**	**1.29**	**0.09**	**19**
	Average diatomite (two-step purification)	**0.66**	**0.05**	**1.34**	**0.07**	**7**
	Diatomite reference value[3]	**0.64**	**0.07**	**1.26**	**0.10**	
14.06.18	BHVO-2F1	−0.13	0.02	−0.28	0.02	
15.06.18	BHVO-2F1	−0.14	0.01	−0.27	0.06	
06.11.18	BHVO-2F1	−0.16	0.03	−0.28	0.02	
07.11.18	BHVO-2F1	−0.16	0.01	−0.21	0.01	
08.11.18	BHVO-2F1	−0.18	0.02	−0.26	0.10	
19.11.18	BHVO-2F1	−0.14	0.03	−0.28	0.03	
07.11.18	BHVO2F2C1	−0.14	0.03	−0.23	0.03	
10.07.18	BHVO2F2C2	−0.15	0.01	−0.22	0.02	
05.02.19	BHVO2F3C1	−0.15	0.01	−0.39	0.03	
08.02.19	BHVO2F3C1	−0.15	0.05	−0.23	0.15	
04.03.19	AnBHVO-2F3C1 400 300[2]	−0.20	0.09	−0.41	0.05	
04.03.19	AnBHVO-2F3C2	−0.19	0.01	−0.36	0.05	
04.03.19	AnBHVO-2F3C3	−0.18	0.03	−0.35	0.09	
	Average BHVO-2 (one-step purification)	**−0.15**	**0.03**	**−0.27**	**0.06**	**10**
	Average BHVO-2 (two-step purification)	**−0.19**	**0.05**	**−0.37**	**0.07**	**3**
	BHVO-2 reference value[4]	**−0.17**	**0.04**	**−0.29**	**0.11**	
09.07.18	QuartzF2C1	−0.01	0.05	0.02	0.05	
06.11.18	QuartzF1	−0.07	0.09	−0.09	0.07	
24.02.19	QuartzF1	0.03	0.05	0.15	0.03	
05.02.19	QuartzF3C1	−0.02	0.04	0.00	0.01	
07.02.19	QuartzF3C1	0.01	0.01	0.02	0.03	
08.02.19	QuartzF3C2	0.00	0.01	0.11	0.07	
15.06.18	AnQuartzF2C1	0.04	0.04	0.05	0.12	
15.06.18	AnQuartzF2C1	0.00	0.01	0.01	0.01	
11.10.18	AnQuartzF2C2	0.02	0.03	0.09	0.01	
09.07.18	AnQuartzF2C3	−0.04	0.04	0.05	0.03	
08.02.19	AnQuartzF3C1	−0.01	0.01	−0.03	0.01	
08.02.19	AnQuartzF3C2	0.00	0.01	0.11	0.04	
22.02.19	AnQuartzF3C4	0.13	0.01	0.07	0.02	
08.02.19	AnQuartzF3C3	0.01	0.01	0.04	0.01	
08.02.19	AnQuartzF3C5	0.08	0.01	−0.03	0.03	
	Average quartz Merck (one-step purification)	**−0.01**	**0.05**	**0.04**	**0.09**	**6**
	Average quartz Merck (two-step purification)	**0.03**	**0.02**	**0.04**	**0.05**	**9**
	Quartz Merck reference value[4]	**0.00**	**0.07**	**−0.01**	**0.12**	

[1] Date of measurement: day of analysis by MC-ICP-MS.

[2] Spiked diatomite or BHVO-2 with X mg.l^{-1} SO_4^{2-} and X mg.l^{-1} Cl^-.

[3] Reynolds et al., 2007.

[4] Abraham et al., 2008.

Appendix F

Plots showing the Ge/Si ratio as a function of the Cl^-/SO_4^{2-} molar ratio (a) and as a function of the Si isotope composition ($\delta^{30}Si$) (b) in the thermal springs. The Ca-SO_4, Ca-Na-Cl and Ca-Na-HCO_3 thermal springs are shown with red, green and blue-filled symbols, respectively. The 2SD error bars reported correspond to ±10% for Ge/Si, and to the largest 2SD value measured on a sample for $\delta^{30}Si$ (Table 2)

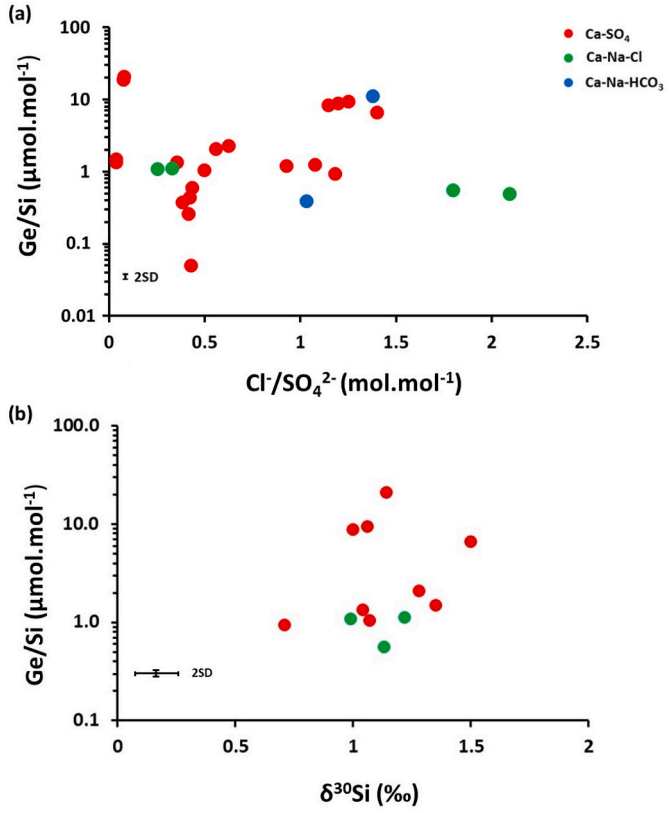

Appendix G

Plots showing the Ge/Si ratio as a function of the concentration in SO_4^{2-} in river water samples. The hydrothermally-impacted rivers (plain triangle) are distinguished from the non-impacted rivers (open triangle). The HI rivers that receive discharges from thermal springs (plain orange triangle) are distinguished from those receiving drainages from an extinct hydrothermal system (plain blue triangle). The NI rivers are displayed according to their locations in Basse-Terre Island: north (open blue triangle), center (open purple triangle), and south (open green triangle). The 2SD error bar reported corresponds to ±10% for Ge/Si. The river codes are explained in Table 1

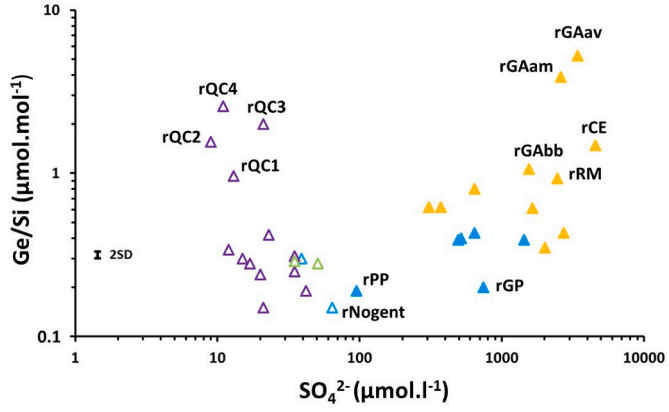

References

Abraham, K., Opfergelt, S., Fripiat, F., Cavagna, A.-J., de Jong, J., Foley, S.F., André, L., Cardinal, D., 2008. δ^{30}Si and δ^{29}Si determinations on USGS BHVO-1 and BHVO-2 reference materials with a new configuration on a Nu Plasma Multi-Collector ICP-MS. Geostand. Geoanal. Res. 32 (2), 193–202.

Aguirre, A.A., Derry, L.A., Mills, T.J., Anderson, S.P., 2017. Colloidal transport in the Gordon Gulch catchment of the Boulder creek CZO and its effect on C-Q relationships for silicon. Water Resour. Res. 53, 2368–2383.

Ameijeiras-Mariño, Y., Opfergelt, S., Derry, L.A., Robinet, J., Govers, G., Minella, J.P., Delmelle, P., 2018. Ge/Si ratios point to increased contribution from deeper mineral weathering to streams after forest conversion to cropland. Appl. Geochem. 96, 24–34.

Arnòrsson, S., 1987. Germanium in Icelandic geothermal systems. Geochim. Cosmochim. Ac. 48, 2489–2502.

Barat, A., 1986. Etude du rôle des eaux souterraines dans le mécanisme des éruptions phréatiques. Application à la Montagne Pelée de Martinique et à la Soufrière de Guadeloupe. BRGM 115.

Baronas, J.J., Torres, M.A., West, A.J., Rouxel, O., Georg, B., Bouchez, J., Gaillardet, J., Hammond, D.E., 2018. Earth Planet. Sci. 503, 194–215.

Baronas, J.J., West, A.J., Burton, K.W., Hammond, D.E., Opfergelt, S., Pogge von Strandmann, P.A.E., James, R.H., Rouxel, O.J., 2020. Ge and Si isotopes behaviour during intense tropical weathering. Global Biogeochem. Cy. https://doi.org/10.1029/2019gb006522.

Bern, C., Brzezinski, M., Beucher, C., Ziegler, K., Chadwick, O., 2010. Weathering, dust, and biocycling effects on soil silicon isotope ratios. Geochim. Cosmochim. Acta 74, 876–889.

Berner, R.A., Lasaga, A.C., Garrels, R.M., 1983. The carbonate-silicate geochemical cycle and its effect on atmospheric carbon-dioxide over the past 100 million years. Am. J. Sci. 283, 641–683.

Bernstein, L.R., 1985. Germanium geochemistry and mineralogy. Geochim. Cosmochim. Ac. 49, 2409–2422.

Bigot, S., Hammouya, G., 1982. Chemistry of the Soufrière of Guadeloupe hot springs. S. E.A.N. Bull 7, 2.

Blazina, T., Sharma, M., 2013. Chemical weathering on the North Island of New Zealand: CO_2 consumption and fluxes of Sr and Os. Geochem. Geophys. Geosyst. 14, 3600–3615.

Boudon, G., Komorowski, J.-C., Villemant, B., Semet, M.P., 2008. A new scenario for the last magmatic eruption of La Soufrière de Guadeloupe (Lesser Antilles) in 1530 A.D.: evidence from stratigraphy, radiocarbon dating and magmatic evolution of erupted products. J. Volcanol. Geotherm. Res. 178, 474–490.

Brombach, T., Marini, L., Hunziker, J.C., 2000. Geochemistry of the thermal springs and fumaroles of Basse-Terre Island, Guadeloupe, Lesser Antilles. B. Volcanol. 61 (7), 477–490.

Brzezinski, M.A., Jones, J.L., Bidle, K.D., Azam, F., 2003. The balance between silica production and silica dissolution in the sea: insights from Monterey Bay, California, applied to the global data set. Limnol. Oceanogr. 48, 1846–1854.

Buss, H., White, A., Dessert, C., Gaillardet, J., Blum, A., Sak, P., 2010. Depth profiles in a tropical volcanic critical zone observatory: Basse-Terre, Guadeloupe. In: Torres-Alvarado, I.S., Birkkle, P. (Eds.), Proceedings of the 13th International Conference on Water–Rock Interaction. Taylor & Francis Group, London, UK.

Cabidoche, Y.-M., Achard, R., Cattan, P., Clermont-Dauphin, C., Massat, F., Sansoulet, J., 2009. Long-term pollution by chlordecone of tropical volcanic soils in the French West Indies: a simple leaching model accounts for current residue. Environ. Pollut. 157, 1697–1705.

Cabidoche, YM., 2011. In: Maurizot, P., Théveniaut, H, Lecomte, P, Cabidoche, YM (Eds.), Sols tropicaux des Outre-mer français tropicaux : une diversité ordonnée par la géochimie de l'altération des roches. Enjeux géologiques propres aux.

Cardinal, D., Alleman, L.Y., De Jong, J., Ziegler, K., André, L., 2003. Isotopic composition of silicon measured by multicollector plasma source mass spectrometry in dry plasma mode. J. Anal. Atom. Spectrom. 18, 213–218.

Chaperon, P., L'Hote, Y., Vuillaume, G., 1985. Les ressources en eau de surface de la Guadeloupe. Editions de l'ORSTOM, Collection Monographies Hydrologiques 7, France.

Chen, X.-Y., Chafetz, H.S., Lapen, T.J., 2020. Silicon isotope variations in hydrothermal systems at Yellowstone National Park, Wyoming, USA. Geochim. Cosmochim. Ac. 283, 184–200.

Clergue, C., Dellinger, M., Buss, H.L., Gaillardet, J., Benedetti, M.F., Dessert, C., 2015. Influence of atmospherics deposits and secondary minerals on Li isotopes budget in a highly weathered catchment, Guadeloupe (Lesser Antilles). Chem. Geol. 414, 28–41.

Colmet-Daage, F., 1969. Cartes des sols des Antilles: Guadeloupe volcanique et Martinique au 1/20 000 (ORSTOM Antilles).

Colmet-Daage, F., Lagache, P., 1965. Caractéristiques de quelques groupes de sols dérivés de roches volcaniques aux Antilles françaises. Cah. L'ORSTOM Ser. Pédologie 8, 91–121.

Cornelis, J.T., Delvaux, B., Cardinal, D., André, L., Ranger, J., Opfergelt, S., 2010. Tracing mechanisms controlling the release of dissolved silicon in forest soil solutions using Si isotopes and Ge/Si ratios. Geochim. Cosmochim. Ac. 74, 3913–3924.

de Hoog, J.C.M., van Bergen, M.J., Jacobs, M.H.G., 2005. Vapour-phase crystallisation of silica from SiF4-bearing volcanic gases. Ann. Geophys. 48, 4/5.

De La Rocha, C.L., Brzezinski, A., DeNiro, M.J., 1996. Purification, recovery and laser-driven fluorination of silicon from dissolved and particulate silica for the measurement of natural stable isotope abundances. Anal. Chem. 68, 3746–3750.

DeArgollo, R., Schilling, J.G., 1978. Ge-Si and Ga-Al fractionation in Hawaiian volcanic rocks. Geochim. Cosmochim. Acta 42, 623–630.

Delvigne, C., Opfergelt, S., Cardinal, D., Delvaux, B., André, L., 2009. Distinct silicon and germanium pathways in the soil-plant system: evidence from banana and horsetail. J. Geophys. Res. 114, G02013.

Delvigne, C., Angeletti, B., Guihou, A., Basile-Doelsch, I., Meunier, J.D., 2018. Reliable determination of Ge in solid environmental samples using a chemical preparation procedure developed for Si isotopes and ICP-MS Analysis. Geostand. Geoanal. Res. 42, 139–149.

Derry, L.A., Kurtz, A.C., Ziegler, K., Chadwick, O.A., 2005. Biological control of terrestrial silica cycling and export fluxes to watersheds. Lett. Nature 433, 728–731.

Dessert, C., Dupré, B., Gaillardet, J., François, L.M., Allègre, C.J., 2003. Basalt weathering laws and the impact of basalt weathering on the global carbon cycle. Chem. Geol. 202, 257–273.

Dessert, C., Gaillardet, J., Dupré, B., Schott, J., Pokrovsky, O.S., 2009. Fluxes of high- versus low-temperature water-rock interactions in aerial volcanic areas: example from the Kamchatka Peninsula, Russia. Geochim. Cosmochim. Ac. 73, 148–169.

Dessert, C., Lajeunesse, E., Lloret, E., Clergue, C., Crispi, O., Gorge, C., Quidelleur, X., 2015. Controls on chemical weathering on a mountainous volcanic tropical island: Guadeloupe (French West Indies). Geochim. Cosmochim. Ac. 171, 216–237.

Dessert, C., Clergue, C., Rousteau, A., Crispi, O., Benedetti, M.F., 2020. Atmospheric contribution to cations cycling in highly weathered catchment, Guadeloupe (Lesser Antilles). Chem. Geol. 531, 119354.

Ding, T.P., Jiang, S., Li, Y., Gao, J., Hu, B., 2017. Geochemistry of Silicon Isotopes. De Gruyter.

Dixon, J.L., Heimsath, A.M., Amundson, R., 2009. The critical role of climate and saprolite weathering in landscape evolution. Earth Surf. Process. Landf. 34, 1507–1521.

Douthitt, C.B., 1982. The geochemistry of the stable isotopes of silicon. Geochim. Cosmochim. Acta 46, 1449–1458.

Escoube, R., Rouxel, O.J., Edwards, K., Glazer, B., Donard, O.F.X., 2015. Coupled Ge/Si and Ge isotope ratios as geochemical tracers of seafloor hydrothermal systems: Case studies at Loihi Seamount and East Pacific rise 9°50'N. Geochim. Cosmochim. Ac. 167, 93–112.

Evans, M.J., Derry, L.A., 2002. Quartz control of high germanium/silicon ratios in geothermal waters. Geology 30, 1019–1022.

Favier, A., Lardeaux, J.-M., Legendre, L., Verati, C., Philippon, M., Corsini, M., Münch, P., Ventalon, S., 2019. Tectono-metamorphic evolution of shallow crustal levels within active volcanic arcs. Insights from the exhumed Basal complex of Basse-Terre (Guadeloupe, French West Indies). Earth Sci. Bull. 190, 10.

François, L.M., Walker, J.C.G., 1992. Modelling the Phanerozoic carbon cycle and climate: constraints from the $^{87}Sr/^{86}Sr$ isotopic ratio of seawater. Am. J. Sci. 292, 81–135.

Frei, R., Polat, A., 2007. Source heterogeneity for the major components of 3.7 Ga Banded Iron Formations (Isua Greenstone Belt, Western Greenland): Tracing the nature of interacting water masses in BIF formation. Earth Planet. Sc. Lett. 253, 266–281.

Fries, D.M., James, R.H., Dessert, C., Bouchez, J., Beaumais, A., Pearce, C.R., 2019. The response of Li and Mg isotopes to rain events in a highly-weathered catchment. Chem. Geol. 519, 68–82.

Frings, P.J., Clymans, W., Fontorbe, G., De La Rocha, C.L., Conley, D.J., 2016. The continental Si cycle and its impact on the ocean Si isotope budget. Chem. Geol. 425, 12–36.

Froelich, P.N., Blanc, V., Mortlock, R.A., Chillrud, S.N., Dunstan, W., Udomkit, A., Peng, T.H., 1992. River fluxes of dissolved silica to the ocean were higher during glacials: Ge/Si in diatoms, rivers, and oceans. Paleoceanogr. Paleoclim. 7, 739–767.

Gaillardet, J., Dupré, B., Louvat, P., Allègre, C.J., 1999. Global silicate weathering and CO_2 consumption rates deduced from the chemistry of the large rivers. Chem. Geol. 159, 3–30.

Gaillardet, J., Rad, S., Rivé, K., Louvat, P., Gorge, C., Allègre, C.-J., Lajeunesse, E., 2011. Orography-driven chemical denudation in the Lesser Antilles: evidence for a new feed-back mechanism stabilizing atmospheric CO_2. Am. J. Sci. 311 (851), 894.

Geilert, S., Vroon, P.Z., Keller, N., Gudbrandsson, S., Stefánsson, A., Van Bergen, M.J., 2014. Silicon isotope fractionation during silica precipitation from hot springs waters. Geophys. Res. EGU2014–7951. Abstract EGU 2014.

Geilert, S., Vroon, P.Z., Keller, N., Gudbrandsson, S., Stefánsson, A., Van Bergen, M.J., 2015. Silicon isotope fractionation during silica precipitation from hot-springs waters: evidence from the Geysir geothermal field, Iceland. Geochim. Cosmochim. Acta 164, 403–427.

Georg, R.B., Reynolds, B.C., Frank, M., Halliday, A.N., 2006. New sample preparation techniques for the determination of Si isotopic compositions using MC-ICP-MS. Chem. Geol. 235, 95–104.

Goldsmith, S.T., Carey, A.E., Lyons, W.B., Hicks, D.M., 2008. Geochemical fluxes and weathering of volcanic terrains on high standing islands: Taranaki and Manawatu-Wanganui regions of New Zealand. Geochim. Cosmochim. Ac. 72, 2248–2267.

Goldsmith, S.T., Carey, A.E., Johnson, B.M., Welch, S.A., Lyons, W.B., McDowell, W.H., Pigott, J.S., 2010. Stream geochemistry, chemical weathering and CO_2 consumption potential of andesitic terrains, Dominica, Lesser Antilles. Geochim. Cosmochim. Ac. 74, 85–103.

Hamade, T., Konhauser, K., Raiswell, R., Goldsmith, S., Morris, R., 2003. Using Ge/Si ratios to decouple iron and silica fluxes in Precambrian banded iron formations. Geology 31, 35–38.

Hambrick, G.A., Froelich, P.N., Meinrat, O.A., Lewis, B.L., 1984. Determination of methylgermanium species in natural waters by graphite furnace atomic absorption spectrometry with hydride generation. Anal. Chem. 56, 421–424.

Han, Y., Huh, Y., Derry, L., 2015. Ge/Si ratios indicating hydrothermal and sulphide weathering input to rivers of the Eastern Tibetan Plateau and Mt. Baekdu. Chem. Geol. 410, 40–52.

Heartsill-Scalley, T., Scatena, F.N., Estrada, C., McDowell, W.H., Lugo, A.E., 2007. Disturbance and long-term patterns of rainfall and throughfall nutrient fluxes in a subtropical wet forest in Puerto Rico. J. Hydrol. 333, 472–485.
Henley, R.W., Ellis, A.J., 1983. Geothermal systems, ancient and modern: a geochemical review. Earth Sci. Rev. 19, 1–50.
Huang, K.J., Teng, F.Z., Wei, G.J., Ma, J.L., Bao, Z.Y., 2012. Adsorption-and desorption-controlled magnesium isotope fractionation during extreme weathering of basalt in Hainan Island, China. Earth Planet. Sci. Lett. 359-360, 73–83.
Hughes, H., Delvigne, C., Korntheuer, M., De Jong, J., André, L., Cardinal, D., 2011. Controlling the mass bias introduced by anionic and organic matrices in silicon isotopic measurements by MC-ICP-MS. J. Anal. Spectrom. 26, 1892–1896.
Hurwitz, S., Evans, W.C., Lowenstern, J.B., 2010. River solute fluxes reflecting active hydrothermal chemical weathering of the Yellowstone Plateau Volcanic Field, USA. Chem. Geol. 276, 331–343.
Jochum, K.P., Weis, U., Schwager, B., Stoll, B., Wilson, S.A., Haug, G.H., Andreae, M.O., Enzweiler, J., 2016. Reference values following ISO guidelines for frequently requested rock reference materials. Geostand. Geoanal. Res. 40, 333–350.
Jones, M.T., Hembury, D.J., Palmer, M.R., Tonge, B., Darling, W.G., Loughlin, S.C., 2011. The weathering and element fluxes from active volcanoes to the oceans: a Montserrat case study. Bull. Volcanol. 73, 207–222.
Kleine, B.I., Stefansson, A., Halldorsson, S.A., Whitehouse, M.J., Jonasson, K., 2018. Silicon and oxygen isotopes unravel quartz formation processes in the icelandic crust. Geochem. Perspect. Lett. 7, 5–11.
Komorowski, J.-C., Boudon, G., Semet, M., Beauducel, F., Antenor-Habazac, C., Bazin, S., Hammouya, G., 2005. Guadeloupe. In: Lindsay, J.M., Robertson, R.E.A., Shepherd, J. B., Ali, S. (Eds.), Volcanic Atlas of the Lesser Antilles. Seismic Research Unit, The University of the West Indies, Kingston, Jamaica, pp. 65–102.
Kurtz, A.C., Derry, L.A., Chadwick, O.A., 2002. Germanium-silicon fractionation in the weathering environment. Geochim. Cosmochim. Ac. 66, 1525–1537.
Kurtz, A.C., Lugolobi, F., Salvucci, G., 2011. Germanium-silicon as a flow path tracer: Application to the Rio Icacos watershed. Water Resour. Res. 47, W06516.
Lerman, A., Meybeck, M., 1988. Physical and Chemical Weathering in Geochemical Cycles. Nato Science Series C. 251. Springer, p. 394.
Lloret, E., Dessert, C., Gaillardet, J., Albéric, P., Crispi, O., Chaduteau, C., Benedetti, M., 2011. Comparison of dissolved inorganic and organic carbon yields and fluxes in the watersheds of tropical volcanic islands, examples from Guadeloupe (French West Indies). Chem. Geol. 280, 65–78.
Louvat, P., Allègre, C.J., 1997. Present day denudation rates of the island of Reunion determined by river geochemistry: basalt weathering and mass budgets between chemical and mechanical erosions. Geochim. Cosmochim. Ac. 61, 3645–3669.
Louvat, P., Gislason, S.R., Allègre, C.J., 2008. Chemical and mechanical erosion rates in Iceland as deduced from river dissolved and solid material. Am. J. Sci. 308, 679–726.
Louvat, P., Gaillardet, J., Paris, G., Dessert, C., 2011. Boron isotope ratios of surface waters in Guadeloupe, Lesser Antilles. Appl. Geochem. 26, S76–S79.
Lugolobi, F., Kurtz, A.C., Derry, L.A., 2010. Germanium-silicon fractionation in a tropical, granitic weathering environment. Geochim. Cosmochim. Ac. 74, 1294–1308.
McMahon, M., Regan, F., Hughes, H., 2006. The determination of total germanium in real food samples including Chinese herbal remedies using graphite furnace atomic absorption spectroscopy. Food Chem. 97, 411–417.
MétéoFrance, 2019. Bulletin Climatique, Guadeloupe.
Mortlock, R.A., Froelich, P.N., 1987. Continental weathering of germanium - Ge/Si in the global river discharge. Geochim. Cosmochim. Ac. 51, 2075–2082.
Mortlock, R.A., Froelich, P.N., 1996. Determination of germanium by isotope dilution-hybride generation inductively coupled plasma mass spectrometry. Anal. Chem. Ac. 332, 277–284.
Muhs, D.R., Budahn, J., Skipp, G., Prospero, J.M., Patterson, D., Bettis III, E.A., 2010. Geochemical and mineralogical evidence for Sahara and Sahel dust additions to Quaternary soils on Lanzarote, eastern Canary Islands, Spain. Terra Nova 22, 399–410.
Nicollin, F., Gibert, D., Beauducel, F., Boudon, G., Komoroswski, J.-C., 2006. Electrical tomography of La Soufrière of Guadeloupe volcano: Field experiments, 1D inversion and qualitative interpretation. Earth. Planet. Sc. Lett. 244, 709–724.
Opfergelt, S., Delmelle, P., 2012. Silicon isotopes and continental weathering processes: Assessing controls on Si transfer to the ocean. Compt. Rendus Geosci. 344, 723–738.
Opfergelt, S., Cardinal, D., André, L., Delvigne, C., Bremont, L., Delvaux, B., 2010. Variations of δ^{30}Si and Ge/Si with weathering and biogenic input in tropical basaltic ash soils under monoculture. Geochim. Cosmochim. Ac. 74, 225–240.
Opfergelt, S., Eiriksdottir, E.S., Burton, K.W., Einarsson, A., Siebert, C., Gislason, S.R., Halliday, A.N., 2011. Quantifying the impact of freshwater diatom productivity on silicon isotopes and silicon fluxes: Lake Myvatn, Iceland. Earth Planet. Sc. Lett. 305, 73–82.
Opfergelt, S., Georg, R.B., Delvaux, B., Cabidoche, Y.M., Burton, K.W., Halliday, A.N., 2012a. Silicon isotopes and the tracing of desilication in volcanic soil weathering sequences, Guadeloupe. Chem. Geol. 326-327, 113–122.
Opfergelt, S., Georg, R.B., Delvaux, B., Cabidoche, Y.M., Burton, K.W., Halliday, A.N., 2012b. Mechanisms of magnesium isotope fractionation in volcanic soil weathering sequences, Guadeloupe. Earth. Planet. Sc. Lett. 311-344, 176–185.
Opfergelt, S., Burton, K.W., Pogge von Strandmann, P.A.E., Gislason, S.R., Halliday, A.N., 2013. Riverine silicon isotope variations in glaciated basaltic terrains: implications for the Si delivery to the ocean over glacial-interglacial intervals. Earth. Planet. Sc. Lett. 369-370, 211–219.
Opfergelt, S., Burton, K.W., Georg, R.B., West, A.J., Guicharnaud, R.A., Sigfusson, B., Siebert, C., Gislason, S.R., Halliday, A.N., 2014. Magnesium retention on the soil exchange complex controlling Mg isotope variations in soils, soil solutions and vegetation in volcanic soils, Iceland. Geochim. Cosmochim. Ac. 125, 110–130.
Petit, R.H., Legrand, M., Jankowiak, I., Molinié, J., Asselin de Beauville, C., Marion, G., Mansot, J.L., 2005. Transport of Saharan dust over the Caribbean Islands: study of an event. J. Geophys. Res. 110, D18S09.
Pokrovsky, G.S., Schott, J., 1998. Experimental study of the complexation of silicon and germanium with aqueous organic species: implications for germanium and silicon transport and Ge/Si ratios in natural waters. Geochim. Cosmochim. Ac. 62, 3413–3428.
Rad, S., Allègre, C.J., Louvat, P., 2007. Hidden erosion on volcanic islands. Earth. Planet. Sc. Lett. 262, 109–124.
Rad, S., Rivé, K., Allègre, C.J., 2011. Weathering regime associated with subsurface circulation on volcanic islands. Aquat. Geochem. 17, 221–241.
Raymo, M.E., Ruddiman, W.F., 1992. Tectonic forcing of late Cenozoic climate. Nature 359, 117–122.
Reed, M.H., 1997. Hydrothermal Alteration and its Relationship to Ore Fluid Composition. Geochemistry of Hydrothermal Ore Deposits, 3rd ed. John Wiley and Sons.
Reynolds, B.C., Aggarwal, J., André, L., Baxter, D., Beucher, C., Brzezinski, M.A., Engström, E., Georg, B., Land, M., Leng, M.J., Opfergelt, S., Rodushkin, I., Sloane, H. J., Van den Boorn, S.H.J.M., Vroon, P.Z., Cardinal, D., 2007. An inter-laboratory comparison of Si isotope reference materials. J. Anal. Atom. Spectrom. 22, 561–568.
Ricci, J., Quidelleur, X., Pallares, C., Lahitte, P., 2017. High-resolution K-Ar dating of a complex magmatic system: the example of Basse-Terre Island (French West Indies). J. Volcanol. Geotherm. Res. 345, 142–160.
Rivé, K., Gaillardet, J., Agrinier, P., Rad, S., 2013. Carbon isotopes in the rivers from the Lesser Antilles: origin of the carbonic acid consumed by weathering reactions in the Lesser Antilles. Earth Surf. Proc. Land. 38, 1020–1035.
Rosas-Carbajal, M., Komorowski, J.-C., Nicollin, F., Gibert, D., 2016. Volcano electrical tomography unveils edifice collapse hazard linked to hydrothermal system structure and dynamics. Sci. Rep. 2016 (6), 29899.
Rouxel, O.J., Luais, B., 2017. Germanium isotope Geochemistry. Rev. Mineral. Geochem. 82, 601–656.
Ruzié, L., Auband, C., Moreira, M., Agrinier, P., Dessert, C., Gréau, C., Cripsi, O., 2013. Carbon and helium isotopes in thermal springs of La Soufrière volcano (Guadeloupe, Lesser Antilles): implications for volcanological monitoring. Chem. Geol. 359, 70–80.
Salaün, A., Villemant, B., Gérard, M., Komorowski, J.-C., Agnès, M., 2011. Hydrothermal alteration in andesitic volcanoes: trace element redistribution in active and ancient hydrothermal systems of Guadeloupe (Lesser Antilles). Fuel. Energ. Abstr. 111, 59–83.
Samper, A., Quidelleur, X., Lahitte, P., Mollex, D., 2007. Timing of effusive volcanism and collapse events within an oceanic arc island: Basse-Terre, Guadeloupe archipelago (Lesser Antilles Arc). Earth. Planet. Sc. Lett. 258, 175–191.
Samper, A., Quidelleur, X., Komorowski, J.C., Lahitte, P., Boudon, G., 2009. Effusive history of the Grande Découverte Volcanic complex, southern Basse-Terre (Guadeloupe, French West Indies) from new K–Ar Cassignol-Gillot ages. J. Volcanol. Geotherm. Res. 187, 117–130.
Schopka, H.H., Derry, L.A., Arcilla, C.A., 2011. Chemical weathering, river geochemistry and atmospheric carbon fluxes from volcanic and ultramafic regions on Luzon Island, the Philippines. Geochim. Cosmochim. Ac. 75, 978–1002.
Scribner, A.M., Kurtz, A.C., Chadwick, O.A., 2006. Germanium sequestration by soil: targeting the roles of secondary clays and Fe-oxyhydroxides. Earth and Plan. Sc. 243, 760–770.
Siebert, C., Ross, A., McManus, J., 2006. Germanium isotope measurements of high-temperature geothermal fluids using double-spike hydride generation MC-ICP-MS. Geochim. Cosmochim. Acta 70, 3986–3995.
Teng, F.Z., Li, W.Y., Rudnick, R.L., Gardner, L.R., 2010. Contrasting lithium and magnesium isotope fractionation during continental weathering. Earth Planet. Sci. Lett. 300, 63–71.
Tribovillard, N., Bout-Roumazeilles, V., Riboulleau, A., Baudin, F., Danelian, T., Riquier, L., 2011. Transfer of germanium to marine sediments: insights from its accumulation in radiolarites and authigenic capture under reducing conditions. Some examples through geological ages. Chem. Geol. 282, 120–130.
Trostle, K., Derry, L., Vigier, N., Chadwick, O., 2014. Magnesium isotope fractionation during arid pedogenesis on the Island of Hawaii (USA). Procedia Earth Planet. Sci. 10, 243–248.
van den Boorn, S.H.J.M., Vroon, P.Z., van Bergen, M.J., 2009. Sulfur-induced offset in MC-ICP-MS silicon-isotope measurements. Anal. At. Spectrom. 24, 1111–1114.
Verati, C., Patrier-Mas, P., Lardeaux, J.-M., Bouchot, V., 2014. Timing of geothermal activity in an active island-arc volcanic setting: first 40Ar/39Ar dating from Bouillante geothermal field (Guadeloupe, French West Indies). Geol. Soc. Lond., Spec. Publ. 378, 285–295.
Verati, C., Lardeaux, J.-M., Favier, A., Corsini, M., Philippon, M., Legendre, L., 2018. Arc-related metamorphism in the Guadeloupe archipelago (Lesser Antilles active island arc): first report and consequences. Lithos 320-321, 592–598.
Villemant, B., Hammouya, G., Michel, A., Semet, M.P., Komorowski, J.-C., Boudon, G., Cheminée, J.-L., 2005. The memory of volcanic waters : Shallow magma degassing revealed by halogen monitoring in thermal springs of La Soufrière volcano (Guadeloupe, Lesser Antilles). Earth. Planet. Sc. Lett. 237, 710–728.
Villemant, B., Komorowski, J.-C., Dessert, C., Michel, A., Crispi, O., Hammouya, G., Beauducel, F., De Chabalier, J.-B., 2014. Evidence for a new shallow magma intrusion at La Soufrière of Guadeloupe (Lesser Antilles), Insights from long-term geochemical monitoring of halogen-rich hydrothermal fluids. J. Volcanol. Geotherm. Res. 285, 247–277.
Vörösmarty, C.J., Fekete, B.M., Meybeck, M., Lammers, R.B., 2000. Global system of rivers: its role in organizing continental land mass and defining land-to-ocean linkages. Glob. Biocheochem. Cy. 14, 599–621.

Westercamp, D., 1988. Magma generation in the Lesser Antilles: geological constraints. Tectonophysics 149, 145–163.
White, A.F., Brantley, S.L., 1995. Chemical weathering rates of silicate minerals: an overview. In: White, A.F., Brantley, S.L. (Eds.), Chemical Weathering Rates of Silicate Minerals, 31st, pp. 1–22. Rev. Miner.
Wilson, S.A., 1998. Data Compilation and Statistical Analysis of Intralaboratory Results for AGV - 2 (U.S. Geological Survey Open-File Report).
Yeghicheyan, D., Bossy, C., Bouhnik Le Coz, M., Douchet, C., Granier, G., Heimburger, A., Lacan, F., Lanzanova, A., Rousseau, T.C.C., Seidel, J.-L., Tharaud, M., Candaudap, F., Chmeleff, J., Cloquet, C., Delpoux, S., Labatut, M., Losno, R., Pradoux, C., Sivry, Y., Sonke, J.E., 2013. A compilation of silicon, rare Earth element and twenty-one other trace element concentrations in the natural river water reference material SLRS-5 (NRC-CNRC). Geostand. Geoanal. Res. 37, 449–467.
Yeghicheyan, D., Aubert, D., Coz, M.B.-L., Chmeleff, J., Delpoux, S., Djouraev, I., Granier, G., Lacan, F., Piro, J.-L., Rousseau, T., Cloquet, C., Marquet, A., Menniti, C., Pradoux, C., Freydier, R., da Silva-Filho, E.V., Suchorski, K., 2019. A new interlaboratory characterisation of silicon, rare Earth elements and twenty-two other trace element concentrations in the natural river water certified reference material SLRS-6 (NRC-CNRC). Geostand. Geoanal. Res. 43, 475–496.
Young, E.D., Galy, A., Nagahara, H., 2002. Kinetic and equilibrium mass-dependent isotope fractionation laws in nature and their geochemical and cosmochemical significance. Geochim. Cosmochim. Ac. 66, 1095–1104.
Ziegler, K., Chadwick, O.A., Brzezinski, M.A., Kelly, E.F., 2005. Natural variations of δ^{30}Si ratios during progressive basalt weathering, Hawaiian Islands. Geochim. Cosmochim. Acta 69, 4597–4610.
Zlotnicki, J., Vargemezis, G., Mille, A., Bruère, F., Hammouya, G., 2006. State of the hydrothermal activity of Soufrière of Guadeloupe volcano inferred by VLF surveys. J. Appl. Geophys. 58, 265–249.